Limnetica, 45(2): 345-378 (2026). DOI: 10.23818/limn.45.22
 ISSN: 0213-8409

Late Pleistocene and Holocene environmental and climate reconstruction from Sierra Nevada, Spain

Gonzalo Jiménez-Moreno[1]*, Antonio García-Alix[1], R. Scott Anderson[2], María J. Ramos-Román[1], Jon Camuera[3], José Manuel Mesa-Fernández[1], Francisco J. Jiménez-Espejo[3], Alejandro López-Avilés[1], Marta Rodrigo-Gámiz[1], Charo López-Blanco[1]

[1] Departamento de Estratigrafía y Paleontología, Universidad de Granada, Spain
[2] School of Earth and Sustainability, Northern Arizona University, USA
[3] Instituto Andaluz de Ciencias de la Tierra (IACT), CSIC, Armilla, Spain
[4] Department of Plant Biology, Faculty of Biology, University of Murcia, Spain

Corresponding author: gonzaloj@ugr.es

Received: 30/06/25 Accepted: 23/02/26 Available online: 27/03/26

ABSTRACT

Late Pleistocene and Holocene environmental and climate reconstruction from Sierra Nevada, Spain

Understanding how climate change and human activity affect fragile mountain ecosystems is key to managing these environments under future climate scenarios, including global warming and increased aridity. Paleoecological records provide long-term insights into how ecosystems responded to past climate shifts and human impacts, especially during warm and/or dry phases. We present a multiproxy study of wetland sediments from the Sierra Nevada, southern Spain, using biotic (pollen, charcoal, biomarkers, chironomids, cladocerans) and abiotic (physical, geochemical) analyses to reconstruct environmental, climatic, and anthropogenic changes over the past ~20 000 years. The coldest conditions occurred during the Last Glacial Maximum and the last deglaciation. A marked warming phase in the Early Holocene coincided with maximum summer insolation, with peak humidity and precipitation between ~10 500 and 7000 cal yr BP, indicated by high water runoff, abundant forest taxa, algae, and elevated total organic carbon. Since ~7000 cal yr BP, especially after a transition around 7000–5000 cal yr BP, progressive cooling and aridification became dominant. This is reflected in shifts in aquatic invertebrate assemblages, declining tree cover, increased xerophytic herbs, reduced runoff, and decreased sediment influx. Geochemical evidence also shows increased Saharan dust input, likely linked to vegetation degradation in North Africa. Superimposed on this long-term aridification trend are millennial-scale cold/arid events at ~7500–7200, 6500, 5200, 4500–4200, 3000, and 1200–1000 cal yr BP. Several of these coincide with known Mediterranean droughts and may relate to persistent positive phases of the North Atlantic Oscillation (NAO+), such as during the Medieval Climate Anomaly. Over the past ~3000 years, human impacts have intensified, with evidence of increased fire activity, grazing, cultivation, atmospheric pollution, and reforestation with Pinus, along with widespread *Olea* cultivation at lower elevations.

KEY WORDS: environmental change; climate; human activity; Late Pleistocene; Holocene; Sierra Nevada.

RESUMEN

Reconstrucción ambiental y climática del Pleistoceno tardío y Holoceno de Sierra Nevada, España

Comprender cómo el cambio climático y la actividad humana afectan a los frágiles ecosistemas de montaña es clave para su gestión futura frente al calentamiento global y la creciente aridez. Los registros paleoecológicos permiten evaluar res-

puestas pasadas de los ecosistemas a variaciones climáticas y presiones antrópicas. Este estudio "multiproxy" de sedimentos de humedales de Sierra Nevada utiliza indicadores bióticos (polen, carbón, biomarcadores, quironómidos, cladóceros) y abióticos (análisis físicos y geoquímicos) para reconstruir los cambios ambientales, climáticos y humanos durante los últimos ~20 000 años. Las condiciones más frías se registraron durante el Último Máximo Glacial y la desglaciación. En el Holoceno temprano se produjo un marcado calentamiento, coincidiendo con el máximo de insolación estival. Entre ~10 500 y 7000 años cal BP se alcanzaron niveles máximos de humedad y precipitación, reflejados en un aumento de escorrentía fluvial, expansión forestal, abundancia de algas y altos niveles de TOC. Desde ~7000 años cal BP, especialmente tras una transición entre 7000–5000 años cal BP, se impuso una tendencia hacia el enfriamiento y la aridificación. Se observa en la reducción del bosque, aumento de hierbas xerófitas, cambios en invertebrados acuáticos, menor escorrentía y aporte sedimentario. También aumenta la deposición de polvo sahariano, relacionada con la degradación de la vegetación en el norte de África. Sobre esta tendencia se superponen eventos fríos y secos a escala milenaria (~7500–7200, 6500, 5200, 4500–4200, 3000 y 1200–1000 años cal BP), algunos coincidentes con sequías mediterráneas y fases NAO+ persistentes, como durante la Anomalía Climática Medieval. En los últimos ~3000 años, los impactos humanos se intensifican: más incendios, pastoreo, cultivos, contaminación atmosférica, repoblaciones con Pinus y cultivo extensivo de Olea *en cotas bajas.*

PALABRAS CLAVE: *cambio medioambiental; clima; impacto humano; Pleistoceno tardío; Holoceno; Sierra Nevada.*

INTRODUCTION

Alpine environments are among the most fragile and climate-sensitive ecosystems (Malanson et al., 2019). Recent climate change is driving altitudinal shifts in plant and animal distributions and contributing to biodiversity loss (Thuiller et al., 2005, Gehrig-Fasel et al., 2008, Malanson et al., 2019). These pressures are compounded by increasing drought in the Mediterranean region, both current and projected, which is also expected to intensify wildfire activity (Pausas & Fernández-Muñoz, 2011, Sousa et al., 2015, 2019, Páscoa et al., 2017, IPCC, 2022).

Studying past environmental and climate variability is essential to improve projections of future ecosystem responses. Paleoecological records since the Last Glacial Maximum (LGM, ~20 000 years) offer valuable insights into how mountain ecosystems reacted to past episodes of maximum cold and ice cover to the last deglaciation and warm conditions, accompanied with variations in humidity and aridity (e.g., Camuera et al., 2019). In this context, the wetlands of the Sierra Nevada serve as an ideal natural laboratory: they are remote, relatively undisturbed, highly biodiverse, and preserve well-resolved signals of both natural climate and anthropogenic changes throughout the Late Pleistocene and Holocene.

Lake and wetland sediments capture the environmental impacts of climate change and human activity—such as shifts in organisms, fire frequency, erosion, and pollution—through the accumulation of biological remains, charcoal, biomarkers, sediment textures, and elemental geochemistry (Cohen, 2003). Over the past two decades, our research group has conducted extensive multidisciplinary studies on sediment records from nine wetlands in the Sierra Nevada (Fig. 1; Table 1).

This review synthesizes findings from these studies, focusing on how biotic and abiotic changes in Sierra Nevada wetlands reflect the interplay of climate variability and human influence over time.

MATERIALS AND METHODS

Sierra Nevada Sites

This study is based on a multi-proxy analysis—including lithological, sedimentological, paleontological, charcoal, and geochemical data—from nine radiometrically well-dated Late Pleistocene and Holocene sedimentary records. These records were obtained from wetland sites situated at varying elevations and orientations across the Sierra Nevada region (Fig. 1; Table 1). The sediment cores from lakes and bogs were collected by the authors between 2006 and 2015 (Table 1).

Eight of the studied sites are located above the treeline within the cryoromediterranean vegetation belt, characterized primarily by alpine tundra vegetation. One site is located in

Table 1. Site description of the Sierra Nevada records synthetized in this study. Asterisks (*) indicate information for just the Holocene part of the Padul sedimentary record. In the analyses done, MS includes lithological-sedimentological description and magnetic susceptibility, and palynology includes pollen, spores, algae and NPP. The various organic and inorganic geochemistry analyses are described in the methods section. *Descripción de las localidades de los distintos registros de Sierra Nevada sintetizados en este estudio. Los asteriscos (*) indican información solo para la parte Holocena del registro sedimentario de Padul. En los análisis realizados, "MS" incluye descripción litológico-sedimentológica y susceptibilidad magnética, y "palinología" incluye polen, esporas, algas y NPP. Los diversos análisis geoquímicos orgánicos e inorgánicos se describen en la sección de métodos.* Sites from the Sierra Nevada are: Padul: Padul peat bog, LS: Laguna Seca; BdlR: Borreguil de la Reina; LdlM: Laguna de la Mula; LdlMo: Laguna de la Mosca; LH: Laguna Hondera; BdlV: Borreguil de la Virgen; BdlC: Borreguil de la Caldera; LdRS: Laguna de Río Seco.

	Coordinates and altitude (m a.s.l.)	Site environment	Core length (cm)	Period covered (cal yr BP)	Dating method	Analyses done	References
LdRS	37º02.43''N, 3º20.57'W; 3020 m	Lake	150	0-21 000	21 AMS ^{14}C dates, 1 ^{137}Cs, 1 ^{210}Pb profiles	MS, Palynology, Org. Geochem., Inorg. Geochem., Charcoal, Chironomids, Cladocerans, Diatoms	Anderson et al. (2011), García-Alix et al. (2013, 2020), Jiménez-Espejo et al. (2014), Toney et al. (2020), Jiménez-Moreno et al., (2023), Llodrà-Llabrés et al. (2024), López-Blanco et al. (2024, 2025)
BdlC	37º03'02'' N, 3º19'24'' W; 2992 m	Peatland	56	0-4400	5 AMS ^{14}C dates	MS, Palynology, Org. Geochem., Inorg. Geochem., Charcoal	Ramos-Román et al. (2016), García-Alix et al. (2017)
BdlV	37º03'15''N, 3º 22'40'' W; 2945 m	Peatland	169	0-8200	9 AMS ^{14}C dates	MS, Palynology, Org. Geochem., Inorg. Geochem.	Jiménez-Moreno and Anderson (2012), García-Alix et al. (2012)
LH	37º02.88'N, 3º17.66'W; 2899 m	Lake	83	0-11 000	7 AMS ^{14}C dates	MS, Palynology, Org. Geochem., Inorg. Geochem.	Mesa-Fernández et al. (2018)
LdlMo	37º03'34.88''N, 3º18'52.98''W; 2889 m	Lake	190	0-8300	10 AMS ^{14}C dates, 1 Pu profile	MS, Palynology, Org. Geochem., Inorg. Geochem., Charcoal, Chironomids	Manzano et al. (2019), Jiménez-Moreno et al. (2025)
LdlM	37º3.583'N, 3º25.017'W; 2497 m	Lake	32.5	0-4100	6 AMS ^{14}C dates	MS, Palynology, Org. Geochem., Inorg. Geochem., Charcoal	Jiménez-Moreno et al. (2013)
BdlR	37º07′48"N, 3º16′21"W; 2421 m	Peatland	97	0-2700	5 AMS ^{14}C dates, 1 Pu profile	MS, Org. Geochem., Inorg. Geochem.	López-Avilés et al. (2021)
LS	37º05′53"N, 2º58′05"W; 2259 m	Seasonal Lake	1400	0-15 800	16 AMS ^{14}C dates, 4 OSL dates	MS, Palynology, Org. Geochem., Inorg. Geochem., Microcharcoal	López-Avilés et al. (2022), Jiménez-Moreno et al. (2023)
Padul	37º00'39.77''N, 3º36'14.06''W; 725 m	Lake/Peatland	327*	0-11 000	14 AMS ^{14}C dates*	MS, Palynology, Org. Geochem., Inorg. Geochem., Charcoal	Ramos-Román et al. (2018a, b), Webster (2018), Camuera et al. (2018, 2019), García-Alix et al. (2021), Rodrigo-Gámiz et al. (2022)

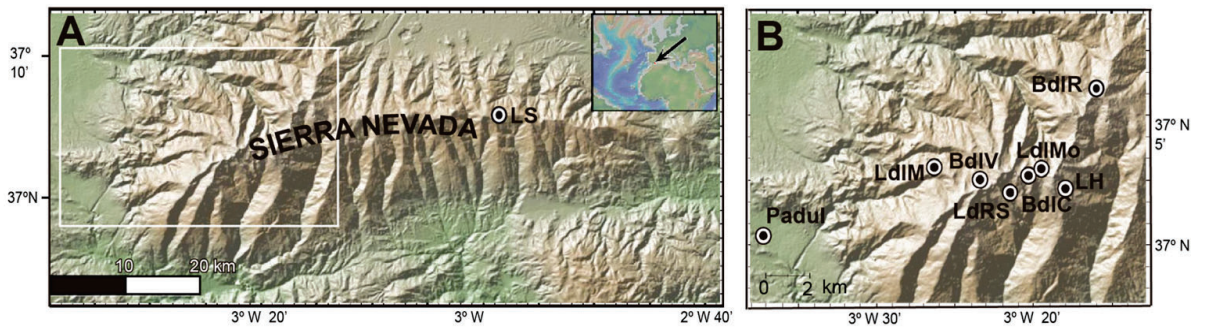

Figure 1. Sierra Nevada wetland site location and photographs. (A) Map of the Sierra Nevada mountain range, southern Iberian Peninsula. The rectangle shows the magnified area shown in (B). (B) Site location of the Sierra Nevada multiproxy records used in this study. *Ubicación y fotografías de los humedales de Sierra Nevada. (A) Mapa de Sierra Nevada, sur de la Península Ibérica. El rectángulo muestra el área ampliada (B). (B) Ubicación de los registros multiproxy de Sierra Nevada utilizados en este estudio*. Site locations: Laguna de Río Seco (LdRS), Borreguil de la Caldera (BdlC), Borreguil de la Virgen (BdlV), Borreguil de la Reina (BdlR), Laguna de la Mosca (LdlMo), Laguna Hondera (LH), Laguna de la Mula (LdlM), Laguna Seca (LS) and Padul-15-05 (Padul). See Table 1 and text for explanation.

the mesomediterranean vegetation belt, where the potential natural vegetation consists mainly of evergreen sclerophyllous oak forests (Valle, 2003).

Four sites—Laguna de la Mula (LdlM) (Jiménez-Moreno et al., 2013), Laguna de la Mosca (LdlMo) (Manzano et al., 2019), Borreguil de la Virgen (BdlV) (García-Alix et al., 2012, Jiménez-Moreno & Anderson, 2012), and Borreguil de los Lavaderos de la Reina (BdlR) (López-Avilés et al., 2021)—are situated on the north-facing slopes of the Sierra Nevada. Another three sites—Laguna de Río Seco (LdRS) (Anderson et al., 2011, García-Alix et al., 2013, 2019, Jiménez-Espejo et al., 2014, Toney et al., 2020, Jiménez-Moreno et al., 2023a, López-Blanco et al., 2024, 2025), Borreguil de la Caldera (BdlC) (Ramos-Román et al., 2016, García-Alix et al., 2017), and Laguna Hondera (LH) (Mesa-Fernández et al., 2018)—are located on the south-facing slopes. The Laguna Seca (LS) site is located facing East (López-Avilés et al., 2022, Jiménez-Moreno et al., 2023b) and the ninth site, the Padul wetland, is situated at the southwestern foothills of the Sierra Nevada (Camuera et al., 2018, 2019, 2021, Ramos-Román et al., 2018a, 2018b, Webster, 2018, García-Alix et al., 2021, Rodrigo-Gámiz et al., 2022).

Together, these sites span a broad altitudinal range—from approximately 725 m asl in the mesomediterranean zone to around 3020 m asl in the cryoromediterranean belt (Table 1).

Sedimentary records: core collection, chronology, lithology, and magnetic susceptibility

Most sediment cores from the alpine sites in the Sierra Nevada were collected using a Livingstone square-rod piston corer, targeting the visual depocenters of each wetland. In lake environments, coring was performed from a floating platform anchored to the shore. The upper 10–20 cm of unconsolidated sediments were retrieved using a universal corer (Aquatic Research Inc.). The LS and Padul-15-05 cores were extracted using a Rolatec RL-48-L drilling rig equipped with a hydraulic piston corer, operated by the Scientific Instrumentation Centre of the University of Granada (CIC-UGR).

All cores were wrapped in plastic and aluminum foil in the field, stored in core boxes, and transported to the laboratory, where they were refrigerated at 4°C for preservation.

Chronologies were established through accelerator mass spectrometry (AMS) radiocarbon dating of plant remains and bulk organic samples. For the uppermost sediment layers, additional dating was conducted using 210Pb, 137Cs, and ICP-MS plutonium profiles (Table 1). Radiocarbon dates were calibrated using the IntCal20 curve (Reimer et al., 2020), and integrated with radionuclide data and the year of core collection

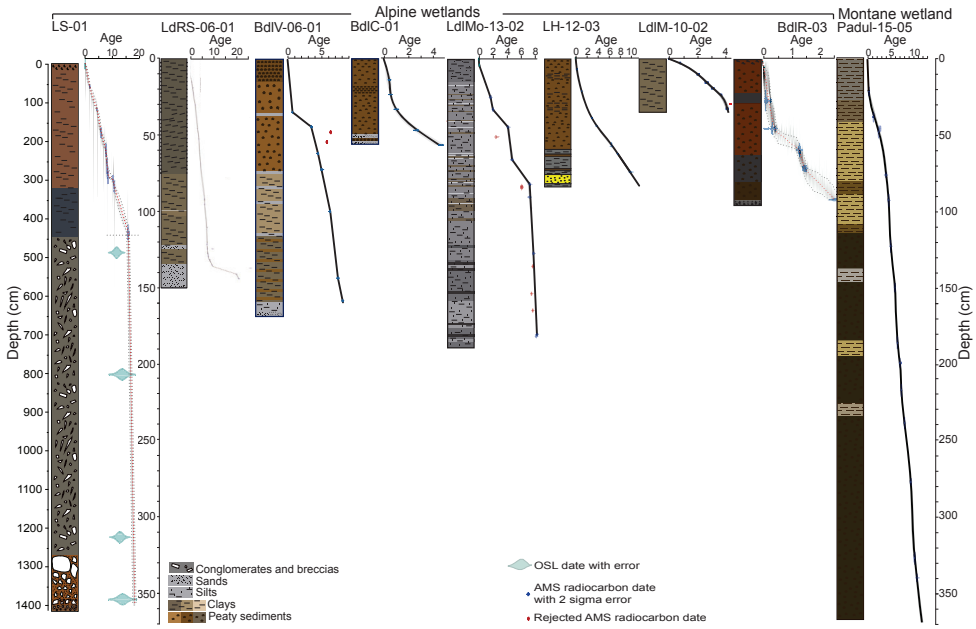

Figure 2. Sediment core lithology and age–depth models for the studied Sierra Nevada records. Red squares are radiocarbon dates that were not used in the age models. *Litología de los testigos de sedimento y modelos de edad-profundidad para los registros estudiados de Sierra Nevada. Los cuadrados rojos son fechas de radiocarbono que no se utilizaron en los modelos de edad*. The studied sites are Laguna Seca (LS-01: LS), Laguna de Río Seco (LdRS-06-01: LdRS), Borreguil de la Virgen (BdlV-06-01:BldV), Borreguil de la Caldera (BdlC-01: BdlC), Laguna de la Mosca (LdlMo-10-02: LdlMo), Laguna Hondera (LH-12-03: LH), Laguna de la Mula (LdlM-10-02: LdlM), Borreguil de la Reina (BdlR-03: BdlR) and Padul (Padul-15-05: Padul). Note that the depth scale for LS-01 is different than the rest of the records. Ages are in cal kyr BP (1 kyr = 1000 years).

to construct robust age–depth models (Fig. 2). In the LS sedimentary record, optically stimulated luminescence (OSL) analyses were also done for the detrital-rich bottom (López-Avilés et al., 2022, Fig. 2).

Age-depth models were developed using either linear interpolation (e.g., BdlV, LdlMo), the smooth spline function in the "clam" software (Blaauw, 2010) for sites such as LdRS, LH, LdlM, and Padul, following the method of Heegaard et al. (2005) on the BdlC site, or calculating a Bayesian age-model using the R-based Bacon package, version 3.1.0 (Blaauw & Christen, 2011) for sites such as, BdlR and LS (see original publications for site-specific details; Table 1). Note that the Padul-15-05 record goes back to almost 200 000 years (Camuera et al., 2019) but for this synthesis we only refer to the latest Pleistocene-Holocene part of the sequence.

Lithological descriptions were based on visual examination of split cores in the laboratory (Table 1; Fig. 2). Magnetic susceptibility (MS), indicating sediment magnetization potential (Snowball & Sandgren, 2001), was measured at 0.5 cm intervals using a Bartington MS2E meter and reported in dimensionless SI units.

Inorganic Geochemistry

Inorganic geochemical analyses of cores from LdRS and LH were conducted at the CIC-UGR using the following methods:

1. Inductively coupled plasma mass spectrometry (ICP-MS) for trace and minor elements.
2. Flame atomic absorption spectrometry (AAS) for major elements in the LdRS core.
3. Inductively coupled plasma optical emission spectrometry (ICP-OES) for major elements in the LH core.

Methodological details are available in Jiménez-Espejo et al. (2014) and Mesa-Fernández et al. (2018).

High-resolution elemental compositions from BdlC, BdlR, LS, LH, and Padul cores were obtained using an Avaatech X-ray fluorescence (XRF) core scanner at the University of Barcelona. Each core was scanned twice using a point sensor: once at 10 s count time (10 kV, 650 μA) for light elements, and again at 35 s count time (30 kV, 1700 μA) for heavier elements. Additional methodological details are provided in García-Alix et al. (2017), Mesa-Fernández et al. (2018), Camuera et al. (2019) and López-Avilés et al. (2021).

Organic geochemistry – bulk sediment and lipid biomarkers analysis

Elemental (C and N) analyses of bulk sediment samples were conducted following acid digestion (to remove carbonates) using a Thermo Scientific Flash 2000 elemental analyzer at CIC-UGR. Carbon isotope ratios were measured using isotope ratio mass spectrometry (IRMS), coupled with elemental analyzers:

- A Carlo Erba Ba 1500 series 2 EA and Thermo Finnigan Delta Plus XL IRMS (IACT-CSIC, Spain) for samples from LdlM, BdlV, and LdRS.
- A Euro EA 300 EA coupled to an Isoprime 50 V IRMS (CIC-UGR) for BdlC samples.

Carbon isotopic values were calibrated with international and internal standards and are expressed in δ notation relative to V-PDB. See García-Alix et al. (2012, 2017), Jiménez-Moreno et al. (2013), Jiménez-Espejo et al. (2014), and Camuera et al. (2019) for further details.

Lipid extractions were carried out using thick slice of freeze-dried sediment samples with an accelerated solvent extractor system Thermo Scientific™ Dionex™ ASE™ 350 using a mixture of dichloromethane:methanol (DCM:MeOH, 9:1, v/v). Total extracts were further separated by silica gel chromatography using polarity-based solvents as described by Rach et al. (2020). n-Alkanes were quantified in the apolar fraction at the BECS Laboratory, University of Glasgow, using gas chromatography with flame ionization detection (GC-FID, Shimadzu 2010). Hydrogen isotopes of sedimentary n-alkanes were analysed with GC- Isotope Ratio Mass Spectrometer (IRMS): a Thermo Fisher Scientific MAT 253™ IRMS coupled to a Thermo Fisher Scientific TRACE GC for the Padul record, and a Finnigan MAT Delta Plus XL IRMS coupled to a HP 6890 GC for the LdRS record. Long-chain diols were analyzed analyzed in the polar fraction previous derivatization with BSTFA on a Shimadzu QP2010 Plus GC-MS in scan and selective ion monitoring (SIM) modes, targeting C28, C30, and C32 diols. See García-Alix et al. (2020) and Toney et al. (2020) for details.

One aliquot of the polar fraction was dissolved in n-hexane:iso-propanol (99:1, v/v) and filtered through a 0.45 mm polytetrafluorethylene (PTFE) filter at the University of Granada. Filtered samples were analysed by ultrahigh performance liquid chromatography/atmospheric pressure chemical ionization-mass spectrometry (UHPLC/APCI-MS) using two UHPLC silica columns (Waters BEH HILIC columns, 2.1 x 150 mm, 1.7 μm) fitted in series following the method described by Hopmans et al. (2016) and using aWaters Acquity UPLC I Class coupled to aWaters XevoTQ-XS triple quadrupole mass spectrometer at CIC-University of Granada.

Palynological Analysis

Pollen analysis followed a modified version of the Faegri & Iversen (1989) protocol. One cm^3 sediment samples were treated with sodium hexametaphosphate (for clay deflocculation), sieved, and chemically processed using HCl, HF, and acetolysis solution. Lycopodium spores were added to calculate pollen concentrations. Residues were mounted in silicone oil (LdRS) or glycerol (all other records) and examined at 400× magnification under a light microscope. A minimum of 300 terrestrial pollen grains were identified per sample, using reference collections from the Universities of Granada, Murcia, and Northern Arizona, as well as modern pollen atlases (e.g., Reille, 1992, Beug, 2004). Pollen percentages were calculated based on the terrestrial pollen sum. Arboreal pollen (AP) was calculated as the percentage of tree pollen rel-

ative to total terrestrial pollen (trees, herbs, and shrubs).

Charcoal Analysis

Macroscopic charcoal analysis was conducted at 0.5 cm intervals in selected cores (LdRS, LdlMo, LdlM, BdlC, Padul). One cm^3 samples were pretreated with sodium hexametaphosphate, then sieved using 250 µm and 125 µm mesh sizes, following the method of Whitlock & Anderson (2003). Charcoal particles were counted under a stereomicroscope (10–70× magnification). Results are reported as charcoal concentrations (CHAC), expressed as the number of charcoal particles per cubic centimeter (particles/cm^3).

Chironomid analysis

Samples of 2 cm^3 from core LdRS-06-01 were processed for chironomid analysis, which involved chemical treatment with sodium hexametaphosphate, sieving at 100-µm, sorting of chironomids from sieve residue at ca. 30x magnification, and taxonomical identification of chironomids on slides with Euparal medium with a light-transmitted microscope at 100x - 400x magnification following Brooks et al. (2007).

Chironomid relative abundances (%) were calculated with respect to the total chironomid count in each sample (Jiménez-Moreno et al., 2023). Based on the fossil chironomid percentage data mean July air temperature estimations were produced using a 274-lake chironomid-temperature calibration dataset and a WA-PLS transfer function from the Swiss Alps and Norway that covers a mean July air temperature gradient from 4 to 18.4 °C and a wide range of arctic, alpine, subalpine and temperate lakes (Heiri et al., 2011).

Cladoceran analysis

Cladoceran analysis was conducted following the protocol outlined by Szeroczynska & Sarmaja-Korjonen (2007). For each analysis, 1 cm^3 of wet sediment was deflocculated in a warm water bath (80 °C) using a 10% potassium hydroxide solution for 30 minutes. The samples were then sieved through a 40 µm mesh. The resulting residue was transferred into test tubes and centrifuged for 10 minutes at 3500 rpm. After centrifugation, the supernatant was decanted, and a small amount of ethanol was added and mixed into the residue. Microscope slides were prepared by placing a drop of liquefied glycerol jelly, stained with a few drops of safranin, onto a heated slide. A cover slip was then carefully placed on top. Samples were examined under a ZEISS Primostar 3 microscope at magnifications of 200–400×. A minimum of 100 individuals were identified and counted per sample (following Kurek et al., 2010), typically ranging between 150 and 400 subfossils (López-Blanco et al., 2024).

For ephippium analysis (Sarmaja-Korjonen, 2003, 2004), both chydorid carapaces (indicative of asexual reproduction) and ephippia (indicative of sexual reproduction) were counted during the routine cladoceran analysis. The relative proportions of ephippia for each species, as well as the Total Chydorid Ephippia (TCE), were calculated. These proportions were based on the number of chydorid carapaces and ephippia, providing a measure of the relative frequency of sexual reproduction among chydorid populations (López-Blanco et al., 2024).

Oxygen-isotope analyses were performed on *Daphnia* ephippia and *Chydorus* carapaces from selected samples from a 150-cm sediment core (LdRS 06–01), covering the last 21 000 calibrated years BP (López-Blanco et al., 2025). Before isotopic analyses, between 30 and 50 *Daphnia* ephippia were digitally photographed and measured in each sample using Image J (Rueden et al., 2017). To avoid altering the isotopic signal of chitin (Verbruggen et al., 2010), pretreatment was limited to water only. Sediments were sieved at 100 µm, and *Daphnia* ephippia and *Chydorus sphaericus* carapaces were manually sorted. Both ephippia and carapaces were thoroughly rinsed multiple times with distilled water and brushed under a stereomicroscope to remove residual mineral or organic matter. Cleaned ephippia were individually separated using soft insect forceps, and all specimens were placed into pre-weighed silver capsules. Oxygen-isotope analyses of cladoceran subfossils were conducted at the Laboratory of Stable Isotopes, CIC-UGR, using a Thermo Fisher Scientific EA IsoLink CNSOH system

coupled to a Delta V Advantage IRMS via a ConFlo IV interface.

Dried samples were weighed to 0.5 ± 0.05 mg using a precision balance, sealed in silver capsules, and introduced into a glassy carbon-filled pyrolysis column via a Zero Blank Autosampler. Pyrolysis was performed at 1430 °C, and the resulting gases were separated chromatographically at 45 °C. Analytical precision was ≤±0.4‰, based on replicate measurements of four nitrogen-rich international standards: USGS42, USGS43, CBS, and KHS. Stable isotope ratios were expressed in standard delta (δ) notation relative to V-SMOW.

RESULTS

Age Control of the Sedimentary Sequences

The age-depth models for the Sierra Nevada sedimentary sequences are based on 93 AMS radiocarbon (^{14}C) dates and four ICP-MS-derived profiles of Plutonium, ^{210}Pb, and ^{137}Cs, which constrain the upper parts of the LdRS, LdlMo and BdlR cores (Fig. 2; Table 1). Four ages from the LS record were obtained using the OSL method (López-Avilés et al., 2022). All dated intervals from the alpine sites from the Sierra Nevada fall within the Late Pleistocene and Holocene (~20 000–0 cal yr BP). The wetland formation and initial sediment deposition across the studied alpine basins follows a three-phase pattern, occurring during deglaciation, ~8200, and ~4200 cal yr BP.

Lithology and Magnetic Susceptibility (MS)

Coring at all alpine Sierra Nevada sites ceased upon encountering coarse sediments, beyond which the manually operated Livingstone corer could not advance. Consequently, the basal portions of many cores are relatively inorganic, with increasing organic content higher in the sequence (Fig. 2). In general, lake cores are composed mainly of silts and clays, while peat dominates the cores from "borreguiles" (peat bogs). Gyttja—very organic-rich clay—is prevalent in LdRS and LdlM. The 190-cm-long LdlMo core is dominated by silty clays with notable variations in grain size and color. The longest alpine sediment record is LS, with a length of more than 14 m. BdlV and LH show similar sequences, with sandy basal layers transitioning through clays to peat-dominated sections in the Middle Holocene (Jiménez-Moreno & Anderson, 2012, Mesa-Fernández et al., 2018). The shorter BdlC and BdlR cores consist of basal sands overlain entirely by peat. The Padul core is characterized by dark, organic-rich peat from ~11 600 to ~7600 cal yr BP, with interspersed clay layers between ~7600 and 4700 cal yr BP, and clay to clayey-carbonate sediments dominating the uppermost ~4700 cal yr BP (Ramos-Román et al., 2018a, b). The LS record, which covers the last ~ 18 000 cal yr BP, is characterized by a paraglacial stage dominated by conglomerate mass flows, (2) a small glacier or nivation hollow stage characterized by breccias and (3) a lacustrine stage between ~ 15 700 cal yr and the present, mostly characterized by lutites. This final stage is interrupted by a periglacial (breccias) substage, probably during the YD (López-Avilés et al., 2022). The thick conglomerate-breccia section of ~10 m deposited in a short time span (Fig. 2) due to paraglacial – small glacier/nivation processes made this sequence the longest recovered alpine core record in the Sierra Nevada.

Magnetic susceptibility (MS) profiles show unique site-specific patterns but also exhibit shared long- and short-term trends across sites (Fig. 3). In the alpine records (e.g., LdRS and LH), Early Holocene MS values are generally high, contrasting with the low MS values recorded at lower elevations in Padul. A marked decline in MS occurred during the Middle Holocene, with some records reaching minima at the transition to the Late Holocene (~5000–4400 cal yr BP). MS values subsequently increased in the Late Holocene, particularly evident in Padul, LH, LdlMo, and LdlM.

Inorganic Geochemistry

Here we summarize key environmental variations in elemental concentrations across the studied sites (Fig. 4; see original publications for detailed datasets). In LH, the Early to Middle Holocene (~11 000 to ~7000 cal yr BP) is marked by elevated K/Ti ratios and low Ca/Al, Ca/Ti, and Zr/Al ratios (Mesa-Fernández et al.,

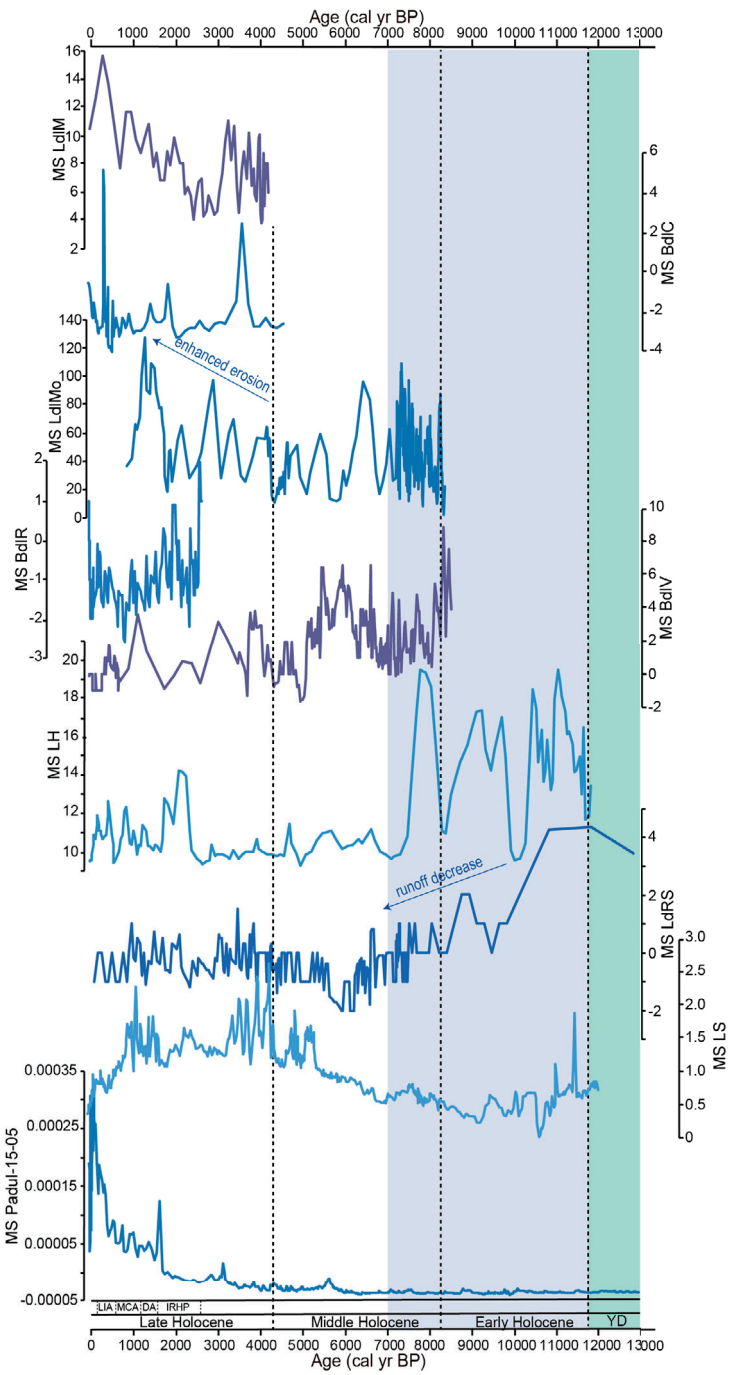

Figure 3. Magnetic susceptibility (MS) records from the Sierra Nevada sediment cores for the last 13 000 cal yr BP. MS data is shown in SI units. YD stands for Younger Dryas (in green shading color). In blue shading is the warmest-wettest period deduced by other climatic proxies discussed in the text and overall highest MS data. IRHP, DA, MCA and LIA stand for Iberian Roman Humid Period, Dark Ages, Medieval Climate Anomaly and Little Ice Age, respectively. *Registros de susceptibilidad magnética (MS) de los testigos de sedimento de Sierra Nevada durante los últimos 13 000 años calibrados BP. Los datos de MS se muestran en unidades del Sistema Internacional (SI). YD significa Dryas Reciente (en verde). En azul se muestra el período más cálido y húmedo deducido por otros indicadores climáticos analizados en el texto y los datos de MS más altos en general. IRHP, DA, MCA y LIA se refieren al Período Húmedo Romano Ibérico, Edad Oscura, Anomalía Climática Medieval y Pequeña Edad de Hielo, respectivamente.*

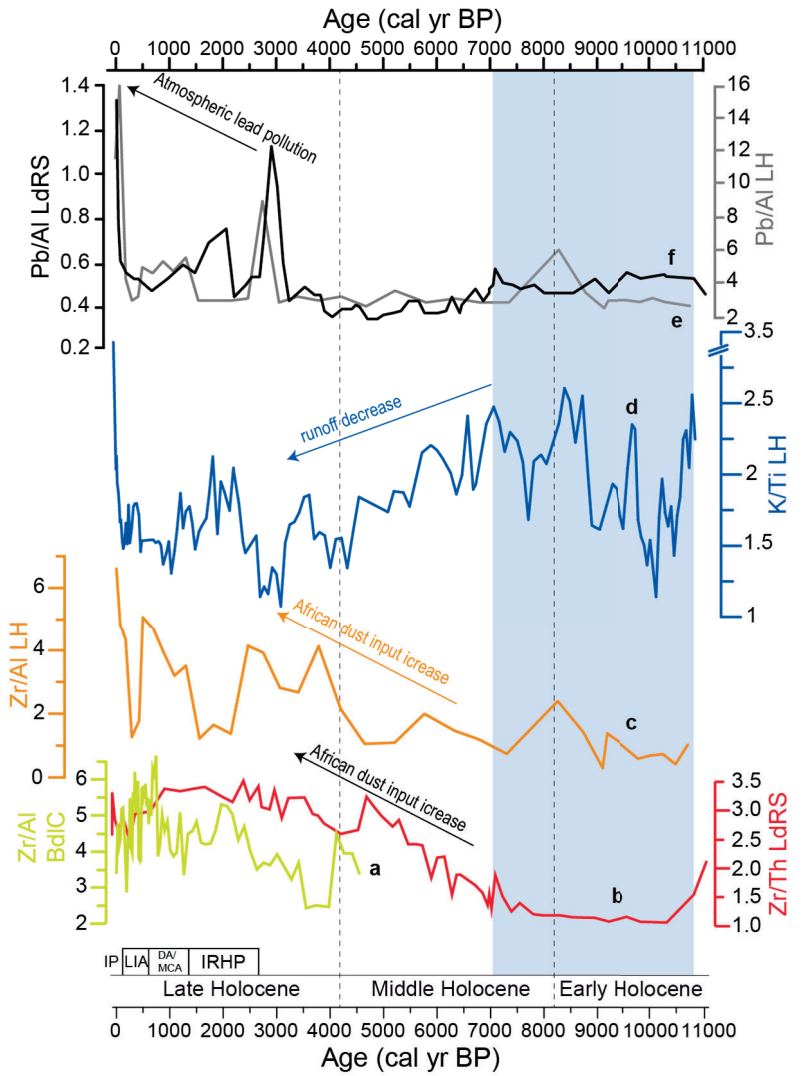

Figure 4. Inorganic geochemistry data from the studied Sierra Nevada wetland sediment records for the last 11 000 cal yr BP. Runoff, lake level and eolian dust proxies. IRHP, DA, MCA, LIA and IP stand for Iberian Roman Humid Period, Dark Ages, Medieval Climate Anomaly, Little Ice Age and Industrial Period, respectively. In blue shading is the wettest period deduced by these and other climatic proxies discussed in the text. *Datos de geoquímica inorgánica de los registros sedimentarios de humedales de Sierra Nevada estudiados durante los últimos 11 000 años cal BP. Análisis de escorrentía, nivel del lago y polvo eólico. IRHP, DA, MCA, LIA e IP corresponden al Periodo Húmedo Ibérico Romano, Edad Oscura, Anomalía Climática Medieval, Pequeña Edad de Hielo y Periodo Industrial, respectivamente. El sombreado azul indica el periodo más húmedo deducido por estas y otras variables climáticas indirectas mencionadas en el texto.* (a) Zr/Al from Borreguil de la Caldera (BdlC; García-Alix et al., 2017). (b) Zr/Th from Laguna de Río Seco (LdRS) (Jiménez-Espejo et al., 2014). (c) Zr/Al from Laguna Hondera (LH) (Mesa-Fernández et al., 2018). (d) K/Ti from Laguna Hondera (LH; Mesa-Fernández et al., 2018). (e) Pb/Al from Laguna Hondera (LH; Mesa-Fernández et al., 2018). (f) Pb/Al from Laguna de Río Seco (LdRS; García-Alix et al., 2013).

2018). Conversely, Zr/Th ratios in LdRS, LH, and BdlC are low during this interval but increase after ~7000 cal yr BP (Jiménez-Espejo et al., 2014, Mesa-Fernández et al., 2018, García-Alix et al., 2017). Pb/Al ratios in LdRS and LH remain low throughout most of the Holocene but show distinct increases during the Late Holocene, peaking around 3000–2500 and 2000 cal yr BP, and again between 1950–1970 AD (García-Alix et al., 2013, Mesa-Fernández et al., 2018).

Organic Geochemistry

C/N ratios in LdRS and BdlV are relatively low

during the Early and Middle Holocene, ranging between ~10 and 16 (Fig. 5). Marked increases are observed at ~6000 cal yr BP (LdRS) and ~5000 cal yr BP (BdlV), with maxima around ~4000 cal yr BP. A general declining trend follows through the Late Holocene. However, both BdlC and BdlV show sharp C/N increases in the last few centuries, followed by a drop in recent decades (except in BdlV, where values remain elevated).

Total Organic Carbon (TOC) in LdRS is low (~2.1%) between ~11 100 and 10 500 cal yr BP, increasing thereafter and peaking (~11.2%) between ~10 500 and 5700 cal yr BP before gradually declining to present-day values (~4.8%) (Fig. 5).

The $\delta^{13}C$ values in BdlV range from –28.1‰ to –23.1‰, averaging –26.4 ± 1.0‰ (V-PDB) (Fig. 5). The highest $\delta^{13}C$ values occur between 8200 and 5100 cal yr BP. A decreasing trend persists from the Middle Holocene to the last 300 years, when values sharply rise.

The Paq index ($C_{21–25}$ *n*-alkanes) from LdRS, indicative of submerged and floating aquatic vegetation, averages 0.37 (range: 0.25–0.48). Paq peaks during the Early Holocene (~11 800–10 500 cal yr BP), increases to a maximum (~0.47) at ~6300 cal yr BP, and then declines until ~260 cal yr BP. A sharp increase occurs over the last ~160 years (Fig. 5).

The Long-chain Diol Index (LDI), calculated from C_{28} and C_{30} diols in LdRS, ranges from 0.05 to 0.31 (mean: 0.18 ± 0.05) (Fig. 5). Elevated LDI values are found at ~5000–4200, ~2540, ~1020, and post-10 cal yr BP. Significant decreases occur at ~6560, ~6170, between ~4100–3900, ~450–150, and ~40–30 cal yr BP. Maximum LDI values are recorded at ~4800–4650 cal yr BP and in the present day.

The distribution of glycerol dialkyl glycerol tetraethers (GDGTs) was analyzed in a sedimentary section spanning the last 36 000 years from the Padul wetland (Rodrigo-Gámiz et al., 2022). The consistently high abundance of branched GDGTs (brGDGTs) relative to crenarchaeol and GDGT-0 indicates predominantly lacustrine (lake-type) environmental conditions, characterized by significant fluctuations in water level. However, the uppermost section of the Padul-15-05 record, corresponding to the last 4700 cal yr BP, shows a distinct shift in GDGT distribution, suggesting a transition to a more ephemeral or periodically emerged lake environment. The GDGT-based reconstructed mean annual air temperatures (MAATs), based on the MBT′$_5$ME index and using the lake-specific calibration of Russell et al. (2018), range between approximately 12 °C and 20 °C for the period between 36 000 and 4700 years before present (Fig. 8). The reconstructed MAAT record from the Padul record indicates cooler conditions during the last three Heinrich Stadials (HS3-1) and the Younger Dryas (YD), and warmer phases during the Dansgaard–Oeschger interstadials (D-O events 7–1) and the Bølling–Allerød (B-A) period. Although the Early and Mid-Holocene are generally characterized by stable and warmer climatic conditions, the Padul record also captures rapid, centennial-scale temperature fluctuations (Rodrigo-Gámiz et al., 2022).

Hydrogen isotopes from plant leaf waxes, more specifically the C_{31} *n*-alkane homologue, can be used as a precipitation proxy in sedimentary archives and were analyzed for the past ~35 000 cal yr BP from Padul and LdRS (Toney et al., 2020, García-Alix et al., 2021). The results show three main periods characterized by different precipitation patterns. Low precipitation, mainly linked to a significant contribution from an isotopically-enriched Mediterranean precipitation source, occurred from ~30 000 to ~15 500 cal yr BP and during the last ~5000 cal yr BP, whereas enhanced precipitation with a predominant isotopically-depleted Atlantic precipitation source prevailed from ~15 500 to ~5000 cal yr BP (García-Alix et al., 2021).

Palynological Analysis

Pollen data indicate that arboreal pollen (AP) was most abundant during the Early and early-Middle Holocene (~11 500–7000 cal yr BP), both in alpine sites (LdRS, BdlV, LdlMo) and at the lower elevation Padul-15-05 site (Fig. 6). Dominant taxa include *Pinus* (likely *P. sylvestris* or *P. nigra*), deciduous *Quercus*, *Betula*, *Alnus*, and *Salix*, while *Artemisia*, *Juniperus*, and Amaranthaceae were less represented. Aquatic algae (*Botryococ-*

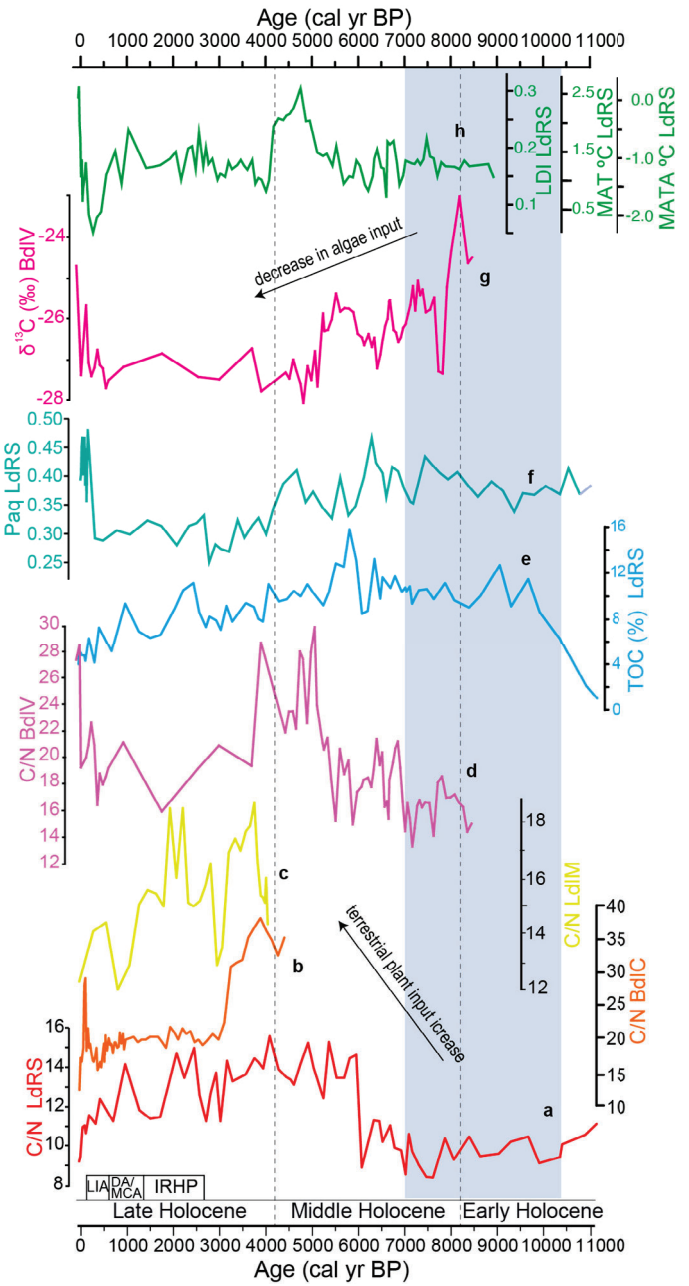

Figure 5. Organic geochemistry data from the studied Sierra Nevada wetland sediment records for the last 11 000 cal yr BP. IRHP, DA, MCA and LIA stand for Iberian Roman Humid Period, Dark Ages, Medieval Climate Anomaly and Little Ice Age, respectively. In blue shading is the wettest period deduced by these and other climatic proxies discussed in the text. *Datos de geoquímica orgánica de los registros sedimentarios de los humedales de Sierra Nevada estudiados durante los últimos 11 000 años cal BP. IRHP, DA, MCA y LIA corresponden al Periodo Húmedo Romano Ibérico, Edad Oscura, Anomalía Climática Medieval y Pequeña Edad de Hielo, respectivamente. El sombreado azul muestra el periodo más húmedo deducido por estas y otras variables climáticas indirectas mencionadas en el texto*. (a) C/N from Laguna de Río Seco (LdRS) (Jiménez-Espejo et al., 2014). (b) C/N ratios from Borreguil de la Caldera (BdlC; Ramos-Román et al., 2016). (c) C/N from Laguna de la Mula (LdlM; Jiménez-Moreno et al., 2013). (d) C/N from Borreguil de la Virgen (BdlV; Jiménez-Moreno & Anderson, 2012). (e) Total organic carbon (TOC) content from Laguna de Río Seco (LdRS; Jiménez-Espejo et al., 2014). (f) Paq from Laguna de Río Seco (LdRS; Toney et al., 2020). (g) □13C from Borreguil de la Virgen (BdlV; García-Alix et al., 2012). (h) LDI record and temperature reconstruction from Laguna de Río Seco (LdRS; García-Alix et al., 2020; Toney et al., 2020).

cus, *Pediastrum*) also peaked during this interval. Between ~7000 and 5000 cal yr BP, forest taxa (especially *Pinus* and deciduous *Quercus*) began to decline, alongside aquatic species. A more marked forest retreat occurred after 5000 cal yr BP, with increases in steppe and ruderal taxa such as *Artemisia*, Amaranthaceae, and Caryophyllaceae. In the last ~950 years, *Olea* expanded, and Pinus recovered, especially during the past few centuries. Fungal spores like *Sporormiella*, an herbivory indicator, increased during the Late Holocene in LdRS (last 3000 years) and in BdlV and BdlC (last 200 years). *Cerealia* pollen and other nitrophilous taxa (*Rumex*, *Plantago*, *Urticaceae*, *Convolvulaceae*) increased significantly over the past ~3000 years, particularly in the last ~1500. Cyclical fluctuations in AP, especially *Pinus* and *Quercus*, are evident, with minima at ~7500, 6500, 5000, 4200, 3000, and 1200 cal yr BP.

Charcoal

Charcoal concentrations in alpine Sierra Nevada Holocene records are generally low (0–20 particles/cm³), peaking at 60 particles/cm³ in LdRS (Anderson et al., 2011; Fig. 7). Only LdRS includes Early Holocene data, indicating low fire activity. Charcoal abundance increases during the Middle Holocene, with peaks at ~6700 and ~5500 cal yr BP in LdRS, and similar peaks (~7500, 6700, 5500 cal yr BP) in LdlMo. During the Late Holocene, charcoal abundance rises in LdRS (from ~3000 cal yr BP onward) and peaks between ~2700 and 1600 cal yr BP in LdlM and BdlC (Fig. 7).

Chironomid analysis

The chironomid-based summer temperature reconstruction from LdRS reveals summer temperature minima over the past 21 000 cal yr BP, corresponding to the Last Glacial Maximum (LGM) and the Younger Dryas (YD) (Jiménez-Moreno et al., 2023; Fig. 8B). A significant warming of approximately 6 °C occurred during the Early Holocene (EH), reaching peak temperatures between ~9000 and 7200 cal yr BP.

From the Middle Holocene through the Late Holocene, a continuous cooling trend is evident, reaching temperature minima around ~1550 and ~200 cal yr BP (~400 and 1750 CE), aligning with the onset of the Dark Ages Cold Period (DA) and the Little Ice Age (LIA) (Jiménez-Moreno et al., 2023, Fig. 8B). The LdRS record shows warmer conditions during the Iberian-Roman Humid Period (IRHP) ~2000 cal yr BP and during the Medieval Climate Anomaly (MCA) at ~1000 cal yr BP. In contrast, the LdRS data show a warming of over 2 °C in recent decades.

Cladoceran analysis

Cladoceran species at the LdRS are characterised by two biological assemblages that shifted their relative abundance at ~5000 cal yr BP. A higher lake-level assemblage characterised by the eurytopic and pioneer *C. sphaericus* dominated samples between 8600 and 5000 cal yr BP. A lower lake-level assemblage composed by taxa associated with vegetation-bare and temporal environments, such as *C. elegans* and *A. quadrangularis*, characterised the upper part of the sequence, between 5000–255 cal yr BP. These biological responses are summarized in RDA axis 1 from the original publication (López-Blanco et al., 2024) and in Fig. 8G.

A comparable change was detected when analysing the ephippium and parthenogenetic carapaces. The Early and Middle-Holocene sediments until ~5000 cal yr BP were generally characterized by lower values of TCE with mean values of ca. 13.5%. Middle and Late-Holocene sediments (~5000 cal yr BP) exhibited oscillations but generally high TCE percentages, with mean values of ca. 26.3%. These results showed a statistically significant increasing trend of sexual reproduction over the Holocene (López-Blanco et al. 2024; Fig. 8G).

Daphnia's mean body (ca. 900 measurements) was between 0.96 and 1.16 mm with the largest body size in the Middle Holocene (~8000–4200 cal yr BP) and a decreasing trend towards the Late Holocene. About their oxygen isotopic composition, $\delta^{18}O$ of *Daphnia* ephippia showed mean values of + 11.82 ‰. Between deglaciation and 4200 cal yr BP, they exhibited generally depleted values only interrupted by a peak at ~ 7200 cal yr BP, concurrent with a temperature maximum in-

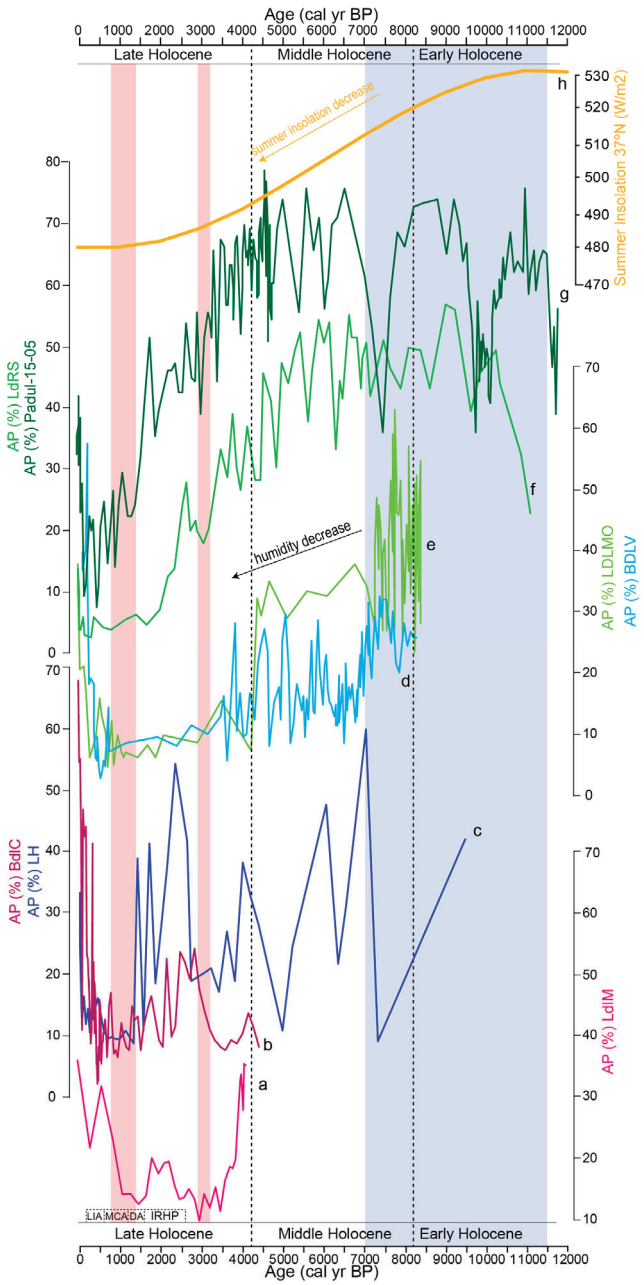

Figure 6. Arboreal pollen (AP) records from the studied Sierra Nevada wetland sediment cores and summer insolation for the last 12 000 cal yr BP. IRHP, DA, MCA and LIA stand for Iberian Roman Humid Period, Dark Ages, Medieval Climate Anomaly and Little Ice Age, respectively. In blue shading is the deduced warmest and wettest period. In red shading are especially arid periods of the Late Holocene that triggered forest reductions. *Registros de polen arbóreo (AP) de los registros sedimentarios de los humedales de Sierra Nevada que han sido estudiados e insolación de verano durante los últimos 12 000 años cal BP. IRHP, DA, MCA y LIA corresponden al Periodo Húmedo Ibérico Romano, Edad Oscura, Anomalía Climática Medieval y Pequeña Edad de Hielo, respectivamente. El sombreado azul representa el periodo más cálido y húmedo deducido. El sombreado rojo representa los periodos especialmente áridos del Holoceno Tardío que desencadenaron la reducción de los bosques*. (a) AP from Laguna de la Mula (LdlM; Jiménez-Moreno et al., 2013). (b) AP from Borreguil de la Caldera (BdlC; Ramos-Román et al., 2016). (c) AP from Laguna Hondera (LH; Mesa-Fernández et al., 2018). (d) AP from Borreguil de la Virgen (BdlV; Jiménez-Moreno & Anderson, 2012). (e) AP from Laguna de la Mosca (Manzano et al., 2019). (f) AP from Laguna de Río Seco (LdRS; Anderson et al., 2011). (g) AP from Padul (Padul-15-05; Ramos-Román et al., 2018a, b). (h) Summer insolation for 37ºN (Laskar et al., 2004).

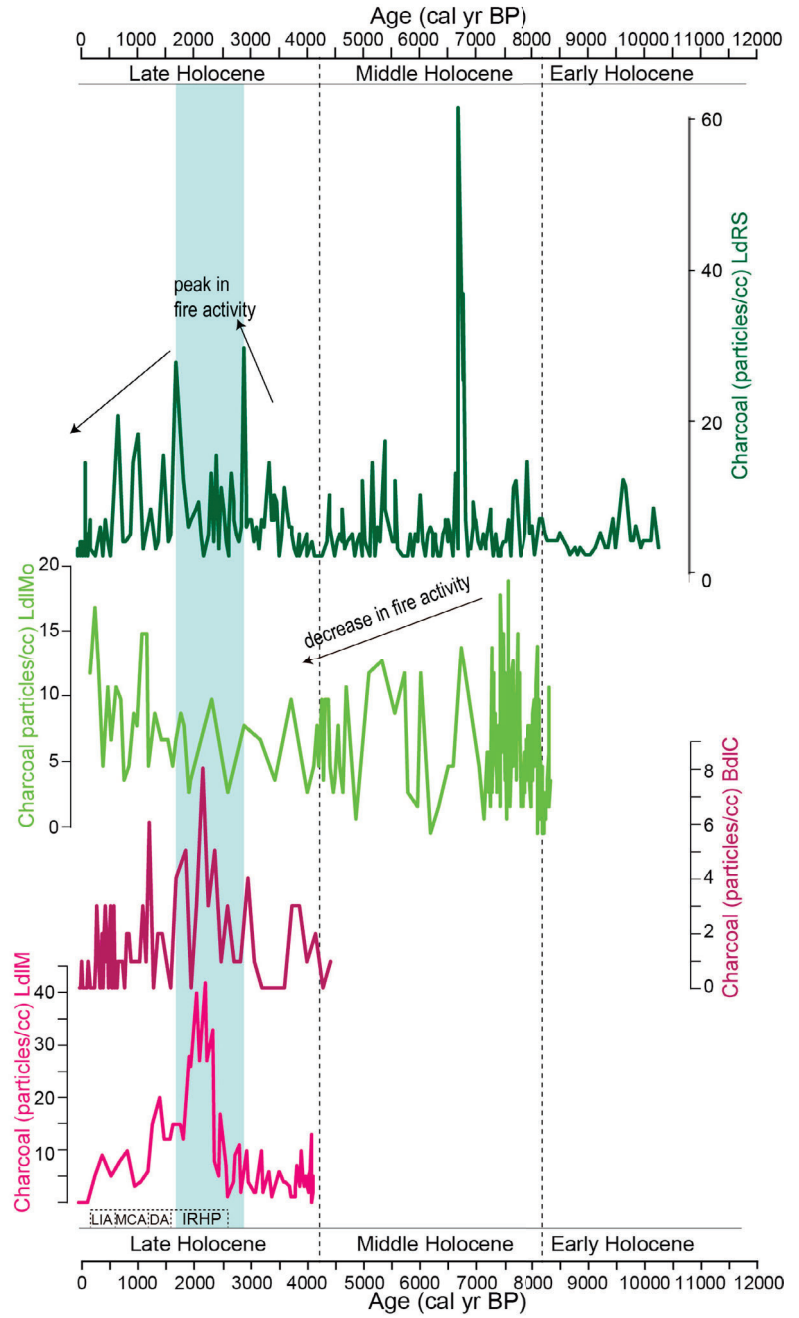

Figure 7. Charcoal records from the studied Sierra Nevada wetland sediment cores indicating fire activity for the last 12 000 cal yr BP. IRHP, DA, MCA and LIA stand for Iberian Roman Humid Period, Dark Ages, Medieval Climate Anomaly and Little Ice Age, respectively. The blue shading highlights an overall increase in charcoal and thus fire activity coinciding with the IRHP. *Registros de carbón vegetal de los testigos sedimentarios de los humedales de Sierra Nevada que han sido estudiados, que indican actividad de incendios durante los últimos 12 000 años cal BP. IRHP, DA, MCA y LIA corresponden al Periodo Húmedo Ibérico Romano, la Edad Oscura, la Anomalía Climática Medieval y la Pequeña Edad de Hielo, respectivamente. El sombreado azul destaca un aumento general de la concentración de carbones y, por lo tanto, de la actividad de incendios, coincidiendo con el IRHP.*

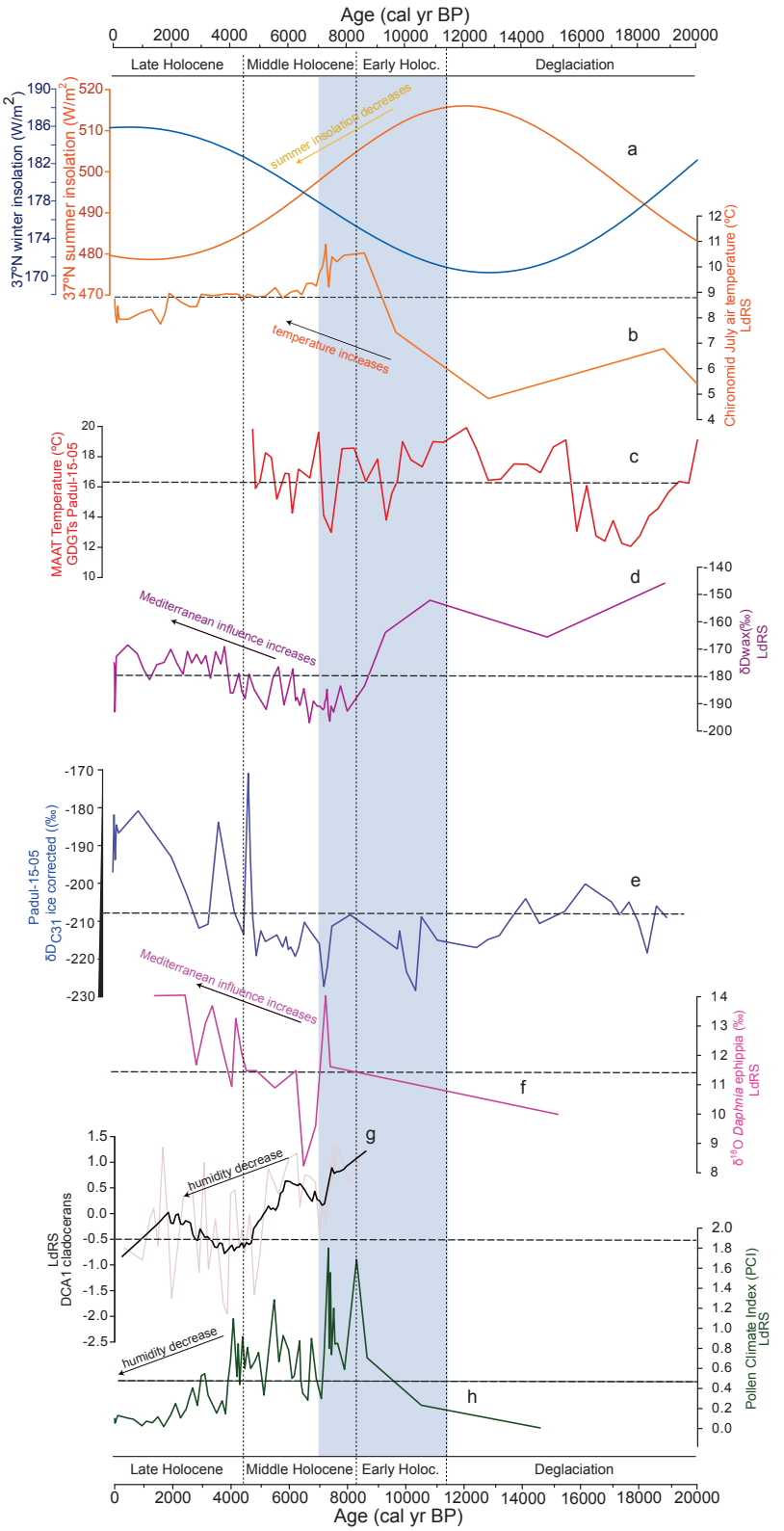
Age (cal yr BP)
0 2000 4000 6000 8000 10000 12000 14000 16000 18000 20000
Late Holocene
Middle Holocene
Early Holoc.
Deglaciation
37°N winter insolation (W/m2)
37°N summer insolation (W/m2)
summer insolation decreases
a
b
temperature increases
Chironomid July air temperature (°C) LdRS
MAAT Temperature (°C) GDGTs Padul-15-05
c
d
Mediterranean influence increases
δDwax(‰) LdRS
Padul-15-05 δDC31 ice corrected (‰)
e
Mediterranean influence increases
f
δ18O Daphnia ephippia (‰) LdRS
g
humidity decrease
LdRS DCA1 cladocerans
humidity decrease
h
Pollen Climate Index (PCI) LdRS

Figure 8. Comparison of paleoclimate proxies from the sedimentary records from Sierra Nevada for the past 20 000 cal yr BP. (a) Summer and winter insolation at 37ºN. (b) Chironomid-based summer temperatures from LdRS (Jiménez-Moreno et al., 2023). (c) Mean annual air temperatures estimated from MBT'5ME based on brGDGTs from Padul record (Rodrigo-Gámiz et al., 2022). (d) Hydrogen isotopic composition of the terrestrial C29 and C31 n-alkanes (δDwax) from LdRS (Toney et al., 2020). (e) δDC31 from Padul (García-Alix et al., 2021). (f) Oxygen isotope stratigraphy (δ18O) of Daphnia ephippia from LdRS. (g) Inferred lake-level changes from cladoceran subfossils from LdRS (López-Blanco et al., 2024). (h) Pollen Climate Index (PCI) from LdRS, calculated from Anderson et al., (2011). Dashed horizontal lines in different proxies are the mean value of the records. The deglaciation sensu lato after Jiménez-Moreno et al. (2023a). In blue shading is the deduced warmest and wettest period. *Comparación de indicadores paleoclimáticos a partir de los registros sedimentarios de Sierra Nevada de los últimos 20 000 años cal BP. (a) Insolación de verano e invierno a 37ºN. (b) Temperaturas de verano basadas en quironómidos de LdRS (Jiménez-Moreno et al., 2023). (c) Temperaturas medias anuales del aire estimadas a partir de MBT'5ME basadas en brGDGT del registro de Padul (Rodrigo-Gámiz et al., 2022). (d) Composición isotópica de hidrógeno de los n-alcanos terrestres C29 y C31 (δDwax) de LdRS (Toney et al., 2020). (e) δDC31 de Padul (García-Alix et al., 2021). (f) Estratigrafía isotópica de oxígeno (δ18O) de Daphnia ephippia de LdRS. (g) Cambios en el nivel del lago inferidos a partir de subfósiles de cladóceros del LdRS (López-Blanco et al., 2024). (h) Índice Climático de Polen (ICP) de LdRS, calculado a partir de Anderson et al. (2011). Las líneas horizontales discontinuas en diferentes indicadores representan el valor medio de los registros. La desglaciación sensu lato se basa en Jiménez-Moreno et al. (2023a). El sombreado azul representa el período más cálido y húmedo deducido.*

ferred from earlier quantitative reconstructions (López-Blanco et al., 2025; Fig. 8). From 4200 cal yr BP onwards, a notable enrichment in this isotopic signal occurred.

DISCUSSION

Age of the sedimentary sequences

Geomorphological evidence indicates that alpine areas above 2000–2200 m asl (north-facing slopes) and 2300–2400 m asl (south-facing slopes) in the Sierra Nevada were glaciated during the last glaciation. Glacial activity carved out the basins where current lakes and bogs now reside (Palacios et al., 2016). Radiocarbon dating of sediment cores from elevations above ~2500 m suggests that wetland formation began shortly after deglaciation (Fig. 2; Table 1). Variable chronological uncertainties may influence inter-site comparisons, but the dating information shows that south-facing sites such as LdRS (3020 m asl) and LH (2899 m asl) show continuous sedimentation since ~20 000 cal yr BP, indicating that the latest Pleistocene warming led to the establishment of wetlands. In contrast, sedimentation in north-facing basins (BdlV at 2945 m asl and LdlMo at 2889 m asl) began later, around ~8200 cal yr BP. Two hypotheses may explain this delay: (1) erosion of early Holocene sediments due to glacial re-advancement during the 8.2 kyr cold event—though no direct glacial evidence supports this in Sierra Nevada (Gómez-Ortiz et al., 2023); or (2) enhanced erosion and coarse sediment deposition during this event buried earlier deposits, which remain unrecovered due to coring limitations. Other sites such as LdlM (2497 m asl, north-facing) and BdlC (2992 m asl, south-facing) show sediment accumulation beginning between ~4400–4100 cal yr BP, possibly linked to aridity generating erosion and/or deposition of coarse sediments during the 4.2 kyr event (e.g., Zielhofer et al., 2019). The absence of older deposits in these basins may reflect either sediment erosion or technical limitations during coring. Once established, sedimentation in these alpine wetlands has been largely continuous (Fig. 2). The Padul basin, at lower elevation, is a graben basin formed in the Early-Middle Pleistocene due to tectonics (Camuera et al., 2019).

Drivers of environment and sedimentary change

Long-term trends observed in the different paleoclimate proxies for the past 20 000 years in Sierra Nevada are mostly consequence of changes in external climate forcings, such as orbital-scale changes in insolation (e.g., Camuera et al., 2019, García-Alix et al., 2021, Rodrigo-Gámiz et al., 2022, Jiménez-Moreno et al., 2023; Fig. 8). Shorter term changes in sedimentary and other paleoenvironmental proxies are related to multidecadal to centennial-scale variability on the climate system and in the last few millennia to human impact.

The relative proportions of detrital material (and thus magnetic minerals) and organic matter in the sediments play a key role in determining magnetic susceptibility (MS). MS values are generally lower when organic matter is abundant, as organic material is diamagnetic (Dearing, 1999). During the Early Holocene, peaks in MS in LdRS and LH may reflect increased winter precipita-

tion, leading to greater snowpack accumulation (Fig. 3). Coupled with maximum summer insolation, this likely caused extensive snowmelt, resulting in significant runoff, enhanced fluvial erosion, and the transport of detrital material into alpine sedimentary basins. Concurrently, increased evaporation at lower elevations due to higher summer insolation likely contributed to lower lake levels in Padul, promoting the development of marshy vegetation and peat formation, which is reflected in the low MS values of that record (Ramos-Román et al., 2018b, Camuera et al., 2018).

The Middle Holocene is marked by MS minima in alpine basins (see Padul, LS, LdRS and LH), coinciding with still relatively humid conditions and declining summer insolation (Fig. 3). These environmental conditions likely favored the proliferation of vegetation and aquatic algae, leading to a greater accumulation of organic matter relative to detrital input in the sediments. A concurrent reduction in winter precipitation, particularly in snowpack accumulation (Ramos-Román et al., 2018b), may have also contributed to decreased erosion and detrital sedimentation. It is likely that both factors—reduced detrital input and increased organic productivity—played a role during this period.

In the Late Holocene, MS displays an overall increasing trend, which has been interpreted as evidence of enhanced erosion and increased deposition of siliciclastic sediments (see Padul, LS, LH, LdlMo and LdM in Fig. 3). This shift may be attributed to a decline in winter precipitation, progressive aridification, and reduced forest cover, all likely associated with decreasing summer insolation (Jiménez-Moreno & Anderson, 2012, Fletcher et al., 2013). Periods of glacier activity in the highest catchments—around 2800–2700, 1400–1200 cal yr BP, and during the Little Ice Age (1300–1850 CE)—may have further intensified erosion processes in the region (Oliva et al., 2020). Finally, a marked increase in land use enhancing erosion and detritic sedimentation over the last ~1550 cal yr BP in the Padul area (Ramos-Román et al., 2018a) suggests that human activity also played a significant role in altering sedimentation patterns during the Late Holocene.

Late Pleistocene and Holocene inorganic geochemistry: lake-level changes, runoff, and dust deposition driven by climate and human impact

Inorganic geochemical data from Sierra Nevada wetland sedimentary records (Fig. 4) provide valuable insights into lithological changes driven by variations in local depositional environments and the influx of allochthonous materials, such as aeolian dust (Jiménez-Espejo et al., 2014, García-Alix et al., 2018). The alpine wetland drainage basins of the Sierra Nevada are primarily composed of metamorphic mica schists, rich in mica and feldspars, and thus abundant in elements like Si, K, and Al (Camuera et al., 2018). Consequently, elemental ratios such as K/Al and K/Ti serve as reliable proxies for detrital input and surface runoff (Mesa-Fernández et al., 2018, López-Avilés et al., 2021). Despite local environmental heterogeneity, consistent broad-scale patterns emerge across the studied sites, revealing regionally coherent responses to Late Pleistocene and Holocene climatic fluctuations. The Laguna Hondera (LH) and Laguna de Río Seco (LdRS) sites exhibit greater sensitivity to climatic variability. Both records pronounced shifts in lithology, geochemistry and magnetic susceptibility suggesting rapid environmental responses to changes in temperature and moisture availability.

High K/Ti values recorded at Laguna Hondera (LH) between ~11 000 and ~7000 cal yr BP indicate a period of intensified runoff and the wettest climatic conditions during the Early to Middle Holocene (Fig. 3). Concurrently, the low Ca/Al, Ca/Ti, and Zr/Al ratios suggest limited aeolian input, supporting the interpretation of a runoff-dominated sedimentary regime during this time (Mesa-Fernández et al., 2018). From ~7000 cal yr BP onward, a trend toward aridification is evident, as shown by declining K/Ti ratios in the LH and BdlR records (Mesa-Fernández et al., 2018, López-Avilés et al., 2021). This transition is further supported by rising values in Saharan dust proxies such as Zr/Th, Zr/Al, Ca/Al, and Ca/Ti, recorded in LH, LdRS, and BdlC, all of which point to increasing aeolian input during the Middle and Late Holocene (Jiménez-Espejo et al., 2014, García-Alix et al., 2017, Mesa-Fernández et al.,

2018). These ratios effectively trace Saharan dust due to its enrichment in heavy minerals (e.g., zircon, rutile) and carbonates—components absent from local Sierra Nevada lithologies. Such proxies have been widely used to reconstruct aeolian input in both Mediterranean and Atlantic contexts (e.g., Rodrigo-Gámiz et al., 2011, Martínez-Ruiz et al., 2015). The increase in Saharan dust emissions likely reflects a concurrent decline in North African vegetation cover (Jiménez-Espejo et al., 2014).

Atmospheric heavy metal pollution from anthropogenic sources at these high-elevation wetlands has been reconstructed through Pb and Pb/Al ratios in sediment cores (García-Alix et al., 2013, Mesa-Fernández et al., 2018). Pb/Al values remained low for most of the Holocene but showed distinct increases during the Late Holocene, with notable peaks around 3000–2500 and 2000 cal yr BP, and again between 1950–1970 AD. These increases are associated with metallurgical activities, especially during the Late Bronze and Early Iron Ages (~3500–2500 cal yr BP / ~1550–550 cal BC), when lead was used in alloying and in cupellation for silver extraction. The exploitation of lead-rich deposits in southeastern Iberia intensified during this time, particularly linked to the southwestern Iberian Pyrite Belt. A subsequent peak in lead pollution during the Roman Empire (~2100–1700 cal yr BP) aligns with regional sedimentary records and historical documentation (García-Alix et al., 2013). The highest levels of lead pollution in the Sierra Nevada occurred during the mid-20th century (1950–1970 AD), corresponding to widespread use of leaded fuel. Following the transition to unleaded fuels and growing environmental awareness, a marked decline in Pb/Al ratios is evident in the sedimentary record, reflecting a reduction in lead emissions (García-Alix et al., 2013, Mesa-Fernández et al., 2018; Fig. 4).

Spatial variability becomes more pronounced during the last millennium. While all sites indicate changes associated with the MCA and LIA, the timing and magnitude of responses vary (Fig. 4). This may reflect microclimatic differences, catchment-specific hydrological dynamics, and varying degrees of anthropogenic influence. For example, LH and LdRS show clear signs of disturbance likely linked to pastoralism and atmospheric pollution in the past ~3000 years (see Pb/Al in Fig. 4), whereas BdlV and BdlC suggest a more gradual environmental response.

Organic geochemistry—TOC, C/N ratios and biomarker data in relation to temperature and precipitation patterns

Organic geochemistry data from Sierra Nevada wetland sediments—including total organic carbon (TOC), carbon-to-nitrogen atomic ratio (C/N), stable carbon isotopes ($\delta^{13}C$), and specific lipid biomarkers (e.g., n-alkanes and long-chain diols)—provide valuable insights into the origin of organic matter and past biogeochemical cycles (Fig. 5).

TOC content reflects the overall organic matter accumulation and wetland productivity. The C/N ratio serves as a proxy for the source of organic matter in lacustrine sediments (Meyers, 1994, Meyers & Teranes, 2001). Algal material, rich in proteins and low in cellulose, typically shows C/N values near 10, while vascular land plants—poor in protein and high in cellulose—commonly exceed values of 20. Intermediate values suggest a mixed algal–terrestrial origin (Meyers & Ishiwatari, 1993). Similarly, $\delta^{13}C$ values help identify organic matter sources and infer productivity levels (Talbot, 2001). Under normal conditions, $\delta^{13}C$ values of lake algae and C_3 plants are similar. However, vascular plants tend to become enriched in ^{13}C under dry conditions due to increased water-use efficiency (Farquhar et al., 1982), whereas algal blooms enrich the dissolved inorganic carbon pool, resulting in higher $\delta^{13}C$ values in algae (O'Leary, 1988, Wolfe et al., 2001).

The initial stages of the deglaciation were characterized by the lack of terrestrial vegetation, deduced from the lowest % TOC and C/N values in the LS record (López-Avilés et al., 2022). Between approximately 17 700 and 15 700 cal yr BP, the low total organic carbon content (%TOC), combined with a wide range of C/N values (5.3 to 33.5), indicates low overall productivity and a mixed source of organic matter. C/N values exceeding 20 suggest a dominant contribution from terrestrial vascular plants (Meyers, 1994), whereas values below 10 are likely associated

with microbial inputs, including bacteria and/or algae (Tyson, 1995, Meyers, 1994, 2003) (López-Avilés et al., 2022) (Fig. 5).

During the Early to Middle Holocene, low C/N values in Sierra Nevada records (e.g., LdRS and BdlV) indicate a dominance of algal and mixed aquatic/terrestrial organic matter, consistent with high lake levels and humid climatic conditions (Jiménez-Espejo et al., 2014, García-Alix et al., 2017; Fig. 5). Concurrent high $\delta^{13}C$ values in BdlV further suggest elevated algal productivity. A marked increase in C/N values between 6000–5000 cal yr BP signals a shift toward greater terrestrial plant input (Fig. 5). In LdRS, this change reflects lower lake levels and reduced algal productivity. In BdlV, it marks a transition from a lake to a bog, aligned with decreased precipitation and increased evaporation. Similar transitions are observed in other alpine bogs (e.g., BdlC around 4400 cal yr BP), coinciding with reduced arboreal pollen and inferred aridity (Fig. 6). Between 5000–4000 cal yr BP, C/N > 20 and $\delta^{13}C$ values in BdlV indicate a dominance of terrestrial vegetation. After 4000 cal yr BP, decreasing C/N values across all records suggest increased aquatic productivity and episodic wetland reactivation. In the last ~300 years, BdlC and BdlV exhibit sharp C/N increases (Fig. 5). However, while C/N declined in BdlC, LdM, and LdRS in recent decades, it remained relatively stable in BdlV, highlighting heterogeneous wetland responses to climatic variability and landscape history across the Sierra Nevada. These abrupt shifts may reflect an amplification of natural trends by human activity (García-Alix et al., 2017).

n-Alkane distributions—resistant to degradation—inform on vegetation and hydrological dynamics (Ficken et al., 2000, Eglinton & Eglinton, 2008). n-Alkanes with 21–25 carbon atoms, derived from submerged and floating aquatic plants, are quantified using the Paq index (Cranwell, 1984, Ficken et al., 2000). High TOC and Paq values in LdRS during the Early to Middle Holocene reflect peak lake productivity and levels, declining thereafter due to progressive aridification (Jiménez-Espejo et al., 2014, Toney et al., 2020; Fig. 5).

Temperature reconstructions are based on the Long-chain Diol Index (LDI), derived from the fractional abundance of C_{28}–C_{30} 1,13- and 1,15-diols, which has shown a close correlation with sea surface temperatures (Rampen et al., 2014; Fig. 5). In LdRS, LDI closely matches instrumental mean annual temperatures (MAAT) over the past century, validating its use as a paleotemperature proxy (García-Alix et al., 2020). LDI-inferred MAAT anomalies (MAATA) fluctuated around ~2.4 °C during the Holocene (Fig. 5). During the Middle to Late Holocene transition, a notable MAATA temperature peak occurred between ~5000 and 4200 cal yr BP, followed by an abrupt cooling around 4150–4100 cal yr BP, reaching a minimum of −1.5 °C at ~4000 cal yr BP. Late Holocene temperatures remained stable near the mean until 1020 cal yr BP, when they rose to −0.5 °C MAATA during the Medieval Climate Anomaly (MCA; Moreno et al., 2012). This was followed by cooling during the Little Ice Age (LIA), with the coldest value (−2.2 °C MAATA) at ~260 cal yr BP. A warming trend resumed in the 20th century, with a brief decline early in the century (−1.7 °C MAATA), followed by temperature increases consistent with modern global warming (IPCC, 2013, García-Alix et al., 2020).

The GDGT-based reconstructed mean annual air temperatures (MAATs) from the Padul record show millennial-scale temperature variability (Fig. 8). Lower MAATs are associated with Heinrich Stadials (such as HS1, not shown here, see Rodrigo-Gámiz et al., 2022 for details), while warmer conditions correspond to the Bolling-Allerod interstadial, the Last Glacial Maximum (LGM), and the Holocene. These short-term variations closely align with shifts observed in regional Mediterranean forest dynamics, underscoring the sensitivity of the Padul system to abrupt climate changes (Rodrigo-Gámiz et al., 2022). This GDGT-based temperature signal aligns well with the $\delta^{18}O$ record from Greenland's NGRIP ice core and marine sediment records from the Alboran Sea, highlighting the strong climatic coupling between mid- and high-latitudes. These results underscore the sensitivity of the southern Iberian continental archive to both regional and hemispheric-scale climate variability.

Leaf wax hydrogen isotopic ratios (δDC31) from Padul were used to reconstruct paleohydrological changes during the last ~35 000 cal

yr BP in the Sierra Nevada (García-Alix et al., 2021; Fig. 8E). Alternating wetter and drier periods were identified in the record, each associated with varying contributions from different moisture sources. Between approximately 30 000 and 15 500 cal yr BP, and again from ~5000 cal yr BP to the present, overall low precipitation levels accompanied by enriched isotopic values suggest a dominant influence from Mediterranean-sourced precipitation and/or a reduction in Atlantic moisture transport. In contrast, the interval from ~15 500 to 5000 cal yr BP was characterized by a marked increase in precipitation, primarily of Atlantic origin and likely delivered as winter rainfall, which occurred contemporaneously with the African Humid Period (García-Alix et al., 2021). Millennial-scale events with enhanced Atlantic or Mediterranean moisture contributions also occurred during periods dominated by the opposite general pattern—for example, during Heinrich Stadial 1 (HS1) and the Early to Middle Holocene (Fig. 8E). Given the Iberian Peninsula's position along the Atlantic storm track trajectory across the Mediterranean Basin, these fluctuations in precipitation amount and moisture source are best explained by shifts in the behavior of the Atlantic storm tracks. Periods of reduced precipitation in the Iberian Peninsula are likely linked to blocked or displaced storm tracks, during which Mediterranean-sourced, isotopically enriched water vapor contributed more significantly to the overall precipitation (García-Alix et al., 2021).

Palynological analysis: latest Pleistocene and Holocene forest, landscape, and lake-level dynamics in response to climate change and human impact

Palynological records from the Sierra Nevada provide critical insights into latest Pleistocene and Holocene vegetation dynamics, climate variability, and human influence (Fig. 6). Arboreal pollen (AP), especially from Mediterranean tree species, serves as a proxy for regional humidity and forest cover (Anderson et al., 20211, Jiménez-Moreno & Anderson, 2012, Ramos-Román et al., 2016, 2018a, Camuera et al., 2019, Jiménez-Moreno et al., 2023). Increases in AP suggest higher moisture availability and forest expansion toward alpine zones, reflecting warmer and more humid conditions that shifted treeline upward.

Planktonic microalgae (e.g., *Pediastrum, Botryococcus, Debarya, Spirogyra, Zygnema*), wetland angiosperms (e.g., Cyperaceae, Ranunculaceae), and other aquatic organisms (such as the flatworm *Neorhabdocoela*) are strongly influenced by fluctuations in lake level and shoreline extent. Variations in the relative abundance of these taxa across climatically distinct periods provide valuable insights into past changes in lake depth, nutrient availability, and overall productivity (Anderson et al., 2011, Ramos-Román et al., 2016, 2018a, b, Mesa-Fernández et al., 2018, Jiménez-Moreno et al., 2023).

Latest Pleistocene and Early Holocene: climate transition and forest expansion

During the deglaciation, sediment records (e.g., LdRS, LS and Padul) indicate a cold and arid steppe-like environment dominated by *Artemisia*, Amaranthaceae, and *Ephedra*. This is consistent with regional data from Carihüela Cave and marine cores from the Alboran Sea (Fernández et al., 2007, Fletcher et al., 2010). The deepest lake levels occurred in LS during the HS1-B-A transition (Jiménez-Moreno et al., 2023).

Increasing but still low summer insolation probably enhanced ice melting and the glacier retreat in the Sierra Nevada, generating runoff and the formation of a deep lake in LS. Cold conditions also favored little evaporation in the LS area during summer, which further controlled the precipitation/evaporation balance increasing lake levels in the area, such as observed in Padul (Camuera et al., 2018, 2019).

Climate warming occurred in southern Spain, including the Sierra Nevada, and the western Mediterranean area during the B-A due to increasing summer insolation, diminishing the LS and Padul lake levels (Camuera et al., 2019, Jiménez-Moreno et al., 2023). Colder and drier conditions occurred again in the western Mediterranean area during the YD (Jiménez-Moreno et al., 2023). LS lake levels increased, probably due to a decrease in evaporation.

The lower-elevation site of Padul shows an early transition (~11 700–11 000 cal yr BP) to

Mediterranean forest dominance, particularly evergreen and deciduous *Quercus*. Between ~10 500 and 7000 cal yr BP, all pollen records show a peak in tree cover (Fig. 6) and aquatic algae (e.g., *Botryococcus*, *Pediastrum*), indicating maximum humidity and warmth. The elevation of subalpine forests likely reached its Holocene maximum, driven by increased summer insolation and enhanced autumn–winter rainfall, a result of stronger land–sea temperature contrasts (Tuenter et al., 2003, Meijer & Tuenter, 2007). Regional (Burjachs et al., 1997, Fletcher & Sánchez Goñi, 2008) and global studies support our results also showing a humid and warm Early Holocene (Jalut et al., 2009, Brayshaw et al., 2011).

Middle to Late Holocene: aridification and forest decline

After ~7000 cal yr BP, especially post-6000–5000 cal yr BP, the Sierra Nevada experienced progressive forest decline (Fig. 6), an increase in drought-adapted (xerophytic) taxa such as *Artemisia* and Amaranthaceae, and a reduction in aquatic species. These trends reflect growing aridity and cooling, corroborated by regional records (e.g., Sierra de Cazorla, Alboran Sea) and other paleoclimate proxies across the Mediterranean (Jalut et al., 2009, Renssen et al., 2003). Declining lake levels and aquatic species in alpine wetlands also support this aridification (Anderson et al., 2011, Jiménez-Moreno & Anderson, 2012, Jiménez-Moreno et al., 2023).

Millennial-scale climate variability

Superimposed on this long-term aridification are millennial-scale oscillations. Significant forest declines occurred ~7500, 6500, 5000, 4200, 3000, and 1200 cal yr BP (Fig. 6), often linked to persistent droughts recognized at regional and global scales (Ramos-Román et al., 2018b). For instance, the Medieval Climate Anomaly (MCA) is marked by notable aridity in the LdlM record (Jiménez-Moreno et al., 2013). Conversely, periods of increased forest cover align with more humid phases such as the Iberian-Roman Humid Period (IRHP) and the Little Ice Age (LIA), suggesting cyclical variability likely tied to the North Atlantic Oscillation (NAO) (Fig. 6). Persistent NAO+ phases favored arid conditions, while NAO– phases brought wetter climates, especially during the LIA (Trouet et al., 2009, Mesa-Fernández et al., 2018).

Human impact: grazing, cultivation, and forest management

Although climate was the primary driver of vegetation changes, human influence became increasingly evident in the past three millennia. Pollen and spore data show early evidence of grazing (e.g., *Sporormiella*, a dung fungus) and cereal cultivation from ~3000 cal yr BP, becoming more pronounced after ~1500 cal yr BP (Anderson et al., 2011, Jiménez-Moreno & Anderson, 2012; Fig. 9). Indicators of land use—such as Asteraceae Cichorioideae, *Rumex*, *Plantago*, *Urtica*, and other ruderal species and grass-parasitizing fungi spores such as *Tilletia* —suggest intensified anthropogenic disturbance, especially in the last 500 years (e.g., in Padul, see Ramos-Román et al., 2018a; Fig. 9).

Large-scale olive cultivation began around 1000 cal yr BP, expanding significantly during the Industrial Revolution and peaking in the mid-20th century, paralleling national trends in olive oil production (see Ramos-Román et al., 2019; Fig. 9). Similarly, the sharp rise in *Pinus* pollen during the last century reflects human-led reforestation for soil stabilization and forest recovery after historical deforestation (see, for example, Anderson et al., 2011).

Charcoal analysis and fire activity in relation to climate and vegetation dynamics

Charcoal analysis, based on the accumulation of charcoal particles in sedimentary layers, provides insights into past fire activity. Sedimentary layers rich in macroscopic charcoal particles (>100 μm) generally indicate local fires, as such particles are unlikely to travel far from their source (Whitlock & Anderson, 2003).

In the Sierra Nevada, sedimentary records analyzed for charcoal, alongside palynological and geochemical proxies, reveal how fire regimes have been influenced by climate fluctuations

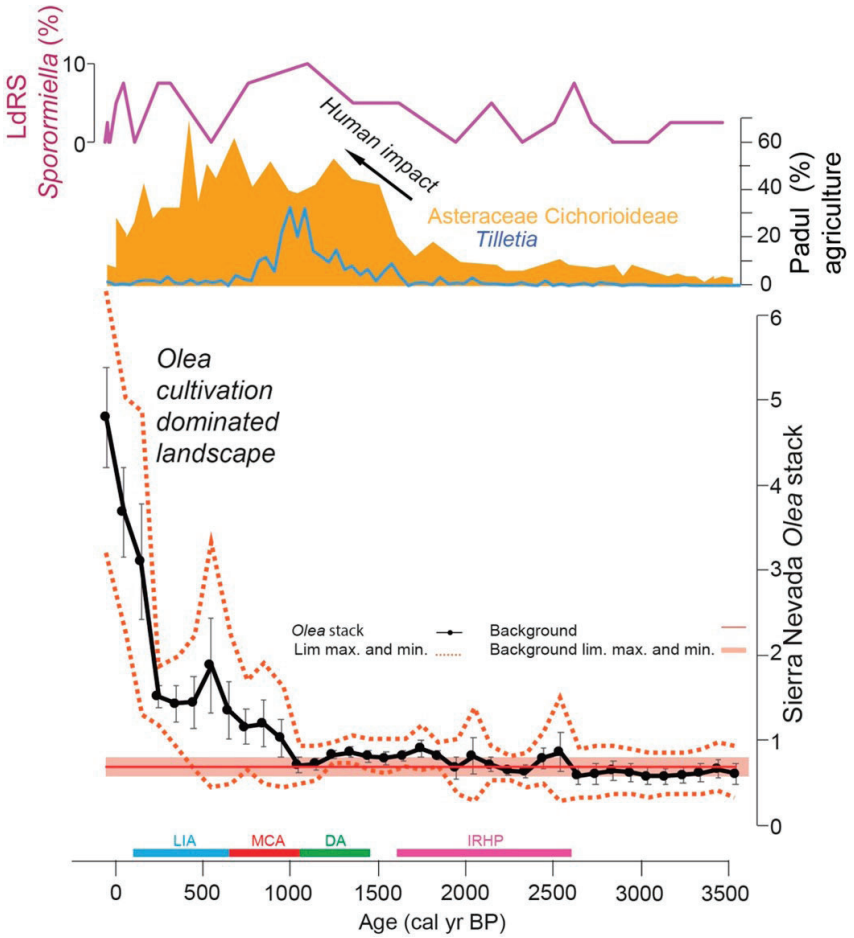

Figure 9. Selection of proxies representing anthropogenic activity in the Sierra Nevada area. At the bottom, synthetic *Olea* stack with error from the Sierra Nevada sites (Ramos-Román et al., 2019). Abundance of nitrophilous plants such as Asteraceae Cichorioideae and the grass-parasitizing fungi *Tilletia* from Padul (Ramos-Román et al.. 2018a). At the top, abundance of herbivore dung fungus *Sporormiella* spores from LdRS (Anderson et al., 2011). *Selección de indicadores que representan la actividad antropogénica en la zona de Sierra Nevada. En la parte inferior, se observa una síntesis de los datos de* Olea*, con su error, de los registros polínicos de Sierra Nevada (Ramos-Román et al., 2019). Abundancia de plantas nitrófilas como Asteraceae Cichorioideae y del hongo parásito de gramíneas,* Tilletia*, de Padul (Ramos-Román et al., 2018a). En la parte superior, abundancia de esporas del hongo herbívoro del estiércol* Sporormiella *de LdRS (Anderson et al., 2011).*

and vegetation changes (Fig. 7). Charcoal concentrations were generally low in alpine zones, likely due to the scarcity of natural fires above the treeline—both in the past and today—and the long-distance transport of charcoal from lower elevations.

Minimum charcoal concentrations recorded during the Late Pleistocene Heinrich Stadial 1 (HS1) at the LS site (Jiménez-Moreno et al., 2023) suggest very low fire activity, likely associated with open pine forests and cold climatic conditions. These low fire frequencies were probably driven by limited fuel availability under cold and arid environmental conditions (Camuera et al., 2019). A slight increase in charcoal during the Bølling–Allerød interstadial (Jiménez-Moreno et al., 2023) may reflect increased fire activity at lower elevations, potentially evidenced by long-distance charcoal transport. This rise in fire occurrence is likely linked to warmer conditions that promoted forest expansion and, consequently, greater fuel availability (Camuera et al., 2019, Daniau et al., 2007). Charcoal particles decreased and show minimum values during the Younger

Dryas at LS, pointing to a decrease in fire activity in the Sierra Nevada lowlands caused by the decrease in temperature and increase in openness of the forest (Camuera et al., 2019). Elevated fire activity is evident during the Middle Holocene (~7500–6700 cal yr BP), due to highest forest fuel occurring in the area, followed by a decline around 7000 cal yr BP. This reduction likely corresponds with decreased forest fuel availability, linked to the retreat of Mediterranean forests and increasing aridity. A notable resurgence in fire activity occurred after ~3000 cal yr BP, peaking between ~2700 and 1600 cal yr BP. This period coincides with the Iberian-Roman Humid Period (IRHP, 2600–1600 cal yr BP)—the most humid phase of the Late Holocene in the region—suggesting that increased humidity led to greater forest density and fuel availability. Similar fire activity peaks during this time are documented across the western Mediterranean, including in the Sierra de Baza, Sierra de Gádor, Alboran Sea, and northern Morocco (Carrión et al., 2003, 2007, Combourieu Nebout et al., 2009, Linstädter & Zielhofer, 2010). These findings support the view that Mediterranean fire regimes are strongly influenced by variations in fuel load, driven by climatic conditions (Daniau et al., 2007). Following the IRHP, charcoal concentrations declined during the Dark Ages and Medieval Climate Anomaly, corresponding with drier, warmer conditions and a reduction in forest cover (Moreno et al., 2012, García-Alix et al., 2020). This aligns with pollen data indicating a retreat of forest species in the Sierra Nevada during this time.

While much of the observed fire activity appears to reflect natural climate variability, increased charcoal accumulation in recent millennia may also result from intensified human activity, including deforestation, mining, agriculture, and grazing (see chapter above and Anderson et al., 2011, García-Alix et al., 2013).

Temperature and hydrological changes deduced by chironomid and cladoceran analyses

The chironomid-based summer temperature reconstruction from LdRS reveals summer temperature minima over the past 21 000 calibrated years BP, corresponding to the Last Glacial Maximum (LGM) and the Younger Dryas (YD) (Jiménez-Moreno et al., 2023; Fig. 8B) and temperature maxima (the HTM) between ~9000 and 7200 cal yr BP. This reflects the strong influence of peak summer insolation during the Early Holocene in high elevation sites (~3000 m a.s.l.) and, amplified by various positive feedback mechanisms. A continuous cooling trend is evident during the Middle and Late Holocene, reaching temperature minima around ~1550 and ~200 cal yr BP (~400 and 1750 CE), aligning with the onset of the Dark Ages Cold Period (DA) and the Little Ice Age (LIA) (Jiménez-Moreno et al., 2023; Fig. 8). This local summer temperature pattern mirrors broader trends in GMST reconstructions (e.g., Kaufman et al., 2020a), which show a gradual decline from the MH to minimum values during the LIA. The rapid warming of over 2 °C in recent decades observed in the LdRS data underscores the exceptional rate of temperature increase currently affecting high-elevation regions of the Sierra Nevada (Jiménez-Moreno et al., 2023; Fig. 8). This temperature reconstruction is consistent with data obtained from dorsal length of fossil *Daphnia* ephippia from the same core, which might have been influenced by the duration of the ice-free season. *Daphnia* ephippia were larger in the Middle Holocene sediments, indicating a longer opening season. The Late Holocene was marked by a shorter opening season, within a gradual cooling at ~4000 cal yr BP inferred by a decrease in ephippia size. Within this period, the smallest remains were measured at ~1572 cal yr BP, coinciding with the Dark Ages Cold Period (DACP) (López-Blanco et al., 2024).

Fluctuations in hydroclimatic variability can be deduced by cladoceran analysis from LdRS, which caused species turnover and changes in the dominant reproduction mode along the Holocene (López-Blanco et al., 2024). A humid phase was identified by a higher lake-level assemblage and lower TCE during the Early and Middle Holocene (~8600–5000 cal yr BP). At that time, the oxygen isotopic data from *Daphnia* ephippia showed a predominantly Atlantic moisture source and changes in the evaporation related to seasonality (Fig. 8F). Conditions became progressively drier since ~5000 cal yr BP, leading to a shift to a lower-level cladoceran assemblage and an increase in

sexual reproduction (higher TCE). An enrichment in the $\delta^{18}O$ isotopic signal of *Daphnia* ephippia occurred since 4200 cal yr BP (Fig. 8F), consistent with a greater influence of a Mediterranean precipitation source and higher evaporation at lower lake levels (López-Blanco et al., 2025).

Regional and Global Comparisons

The environmental trajectories reconstructed from the Sierra Nevada alpine wetlands are broadly consistent with Holocene patterns observed in other Mediterranean and high-altitude regions (e.g., Carrión, 2002, Fletcher et al., 2010, Rodrigo-Gámiz et al., 2014, Samartin et al., 2017, Català et al., 2019), while also exhibiting site-specific responses to climatic and anthropogenic forcings. At a regional scale, the gradual Middle to Late Holocene aridification observed in the Sierra Nevada parallels trends identified across the western Mediterranean, including the Iberian Peninsula (see references above). Proxy evidence from speleothems, lacustrine sediments, and pollen records indicates a widespread shift toward drier conditions, typically attributed to declining summer insolation and a southward displacement of the westerlies (Camuera et al., 2023). The correspondence between these patterns suggests that the Sierra Nevada responded to the same large-scale atmospheric dynamics that shaped the Mediterranean climate during the Holocene.

Globally, the timing of major climatic events—such as variability during the deglaciation (HS1, B-A and YD), the 4.2 kyr aridification pulse, and the LIA—aligns with abrupt environmental changes documented in mid- to high-latitude archives, including Greenland ice cores and North Atlantic marine sediments, and African monsoon records (Camuera et al., 2021, 2022). This synchronicity underscores the global teleconnections that influenced Holocene climate variability, with the Sierra Nevada serving as a sensitive node in these larger climatic networks.

However, differences emerge in the expression and intensity of these events due to local topography, elevation, and catchment characteristics. For example, the hydroclimatic impact of the 4.2 kyr event is more pronounced in lowland Mediterranean basins than in high-altitude Sierra Nevada wetlands, where buffering effects from snowpack and groundwater storage may have moderated ecological responses.

Anthropogenic signals, while increasingly prominent throughout the Holocene, also show geographic variability. In more accessible Mediterranean lowlands, human-induced landscape transformation began earlier and proceeded more intensively, whereas in the Sierra Nevada, anthropogenic imprints become distinctly visible only in the late Holocene (see Alba-Sánchez et al., 2021, Jiménez-Moreno et al., 2022). Nevertheless, during periods such as the IRHP and the MCA, even these remote mountain systems experienced measurable ecological change, reflecting the expansion of land use and transhumance into high-altitude zones.

In summary, the Sierra Nevada record offers a valuable high-resolution complement to broader regional and global Holocene syntheses. It highlights both the coherence of climatic signals across diverse geographic contexts and the importance of local environmental and cultural factors in shaping the timing and magnitude of ecosystem responses.

Implications for future environmental change

The Late Pleistocene and Holocene environmental history reconstructed from the Sierra Nevada wetlands provides critical insights into the resilience and vulnerability of high-mountain ecosystems under varying climatic and anthropogenic pressures. By contextualizing past ecosystem responses within broader climatic regimes, the findings offer important implications for anticipating the trajectory of these systems under future global change scenarios.

Firstly, the paleoecological record highlights the sensitivity of alpine and montane wetlands to shifts in temperature and hydrological regimes (e.g., García-Alix et al., 2020, Jiménez-Moreno et al., 2023). Periods of sustained aridity or increased climatic variability—such as the Late Holocene drying trend and millennial-scale variability such as the IRHP, the MCA or LIA—resulted in marked ecological reorganizations, including changes in vegetation composition,

aquatic productivity, and sedimentary dynamics (e.g., Jiménez-Moreno et al., 2013, Ramos-Román et al., 2018a, b). This suggests that projected future warming and altered precipitation patterns are likely to elicit similarly significant responses, particularly in systems already operating near ecological thresholds.

Secondly, the Late Holocene increase in anthropogenic impact, coinciding with intensified land use, deforestation, and grazing pressure, demonstrates that human activities can amplify or modulate climate-driven environmental changes (Ramos-Román et al., 2016, 2019). In the context of accelerating global change, this dual forcing—climatic and anthropogenic—is expected to exert compound effects on alpine ecosystems, potentially overwhelming their adaptive capacity.

Finally, the Sierra Nevada record contributes to a growing body of evidence that high-elevation environments function as early indicators—or "sentinels"—of climate change. Given their ecological sensitivity, these systems are likely to experience disproportionate impacts from ongoing warming trends. As such, the preservation and monitoring of alpine wetlands should be prioritized within regional conservation frameworks, not only for their intrinsic ecological value but also for their role as critical archives and barometers of environmental change.

CONCLUSIONS

This study presents a synthetic reconstruction of Late Pleistocene and Holocene environmental change in the alpine wetlands of the Sierra Nevada, utilizing a multiproxy paleoenvironmental and palaeoecological approach. By integrating a wide range of analyses including palynology, chironomid and cladoceran analyses, sedimentary, biomarkers and geochemical parameters, and charcoal records, the research reveals complex interactions between climate variability, ecological dynamics, and human influence over the past ~20 000 years.

Minima in temperatures of the last ~20 000 cal yr BP occurred during the LGM, the HS1 and the YD periods. Low precipitation, mainly linked to a significant contribution from an isotopically-enriched Mediterranean precipitation source, also occurred at that time. Temperatures rose significantly during the Early Holocene and the highest temperatures (the HTM) were reached in the Early and Middle Holocene between ~9000 and ~7000 cal yr BP. Higher and Atlantic-source precipitation prevailed then. The Early to Middle Holocene was characterized by relatively stable climatic conditions and limited anthropogenic impact, fostering the development of diverse and resilient wetland communities. In contrast, the late Holocene witnessed increasing climatic variability, particularly episodes of aridity, alongside growing anthropogenic pressure from land-use changes and livestock grazing. These drivers collectively contributed to notable ecological shifts, including reduced aquatic productivity, altered vegetation composition, and increased fire activity.

The findings highlight the high sensitivity of alpine wetland ecosystems to both natural and anthropogenic factors. In this context, the Sierra Nevada serves as a valuable case study for understanding broader patterns of environmental change in Mediterranean high-mountain systems. The palaeoecological insights gained here offer critical context for current and future environmental management. As climate change accelerates and anthropogenic pressures intensify, the resilience of alpine wetlands will likely be further tested. Long-term records such as those presented in this study are essential for informing conservation strategies that anticipate future challenges while recognizing the enduring imprint of past environmental change.

ACKNOWLEDGEMENTS

This study was supported by projects PID2021-125619OB-C21/C22, funded by Ministerio the Ministerio de Ciencia e Innovación of Spain, the Agencia Estatal de Investigación and Fondo Europeo de Desarrollo Regional FEDER MCIN/AEI/10.13039/501100011033/FEDER, UE; BIOD22_001 and BIOD22_002, funded by Consejería de Universidad, Investigación e Innovación and Gobierno de España and Unión Europea – NextGenerationEU; CGL2013-47038-R, CGL2017-85415-R and Séneca Project 20788/PI/18; Junta de Andalucía I+D+i Junta de Anda-

lucía 2020 Retos P-20-00059, FEDER Project B-RNM-144-UGR18, UGR-FEDER B-RNM-144-UGR18 Proyectos I + D + i del Programa Operativo FEDER 2018 and the research group RNM-190 (Junta de Andalucía). M.J.R.R. acknowledges the postdoctoral funding provided by the European Commission/H2020 (ERC-2017-ADG, project number 788616). J.C. acknowledges the postdoctoral funding provided by the Academy of Finland (project number 316702). A.G.-A. acknowledges the Ramón y Cajal fellowship RYC-2015-18966 provided by the Ministerio de Economía y Competitividad of the Spanish Government. M.R.G. acknowledges funding by the Juan de la Cierva-Incorporación program in the University of Granada (IJCI-2017-33755) from Secretaría de Estado de I+D+i, Spain. RSA acknowledges several travel grants from Northern Arizona University to support this work.

AUTHOR CONTRIBUTIONS

G.J.-M., A.G.-A. and R.S.A.: conceived the study; G.J.-M., A.G.-A., R.S.A., M.J.R.-R., J.C., J.M.M.-F., F.J.J.-E. and A.L.-A.: collected field data; G.J.-M., A.G.-A., R.S.A., M.J.R.-R., J.C., J.M.M.-F., F.J.J.-E., A.L.-A., M.R.-G. and C.L.-B: analyzed the data. G.J.-M.: wrote the manuscript with feedback from A.G.-A., R.S.A., M.J.R.-R., J.C., J.M.M.-F., F.J.J.-E., A.L.-A., M.R.-G. and C.L.-B.

REFERENCES

Aba-Sánchez, F., Abel-Schaad, D., López-Sáez, J.A., Sabariego-Ruiz, S., Pérez-Díaz, S., Luelmo-Lautenschlaeger, R. & Garrido-García, J.A. (2021). Early anthropogenic change in western Mediterranean mountains (Sierra Nevada, SE Spain. *Anthropocene*, 33, 100278. DOI: 10.1016/j.ancene.2021.100278

Anderson, R.S., Jiménez-Moreno, G., Carrión, J.S. & Pérez-Martínez, C. (2011). Holocene vegetation history from Laguna de Río Seco, Sierra Nevada, southern Spain. *Quaternary Science Reviews*, 30, 1615–1629. DOI: 10.1016/j.quascirev.2011.03.005

Beug, H.-J. (2004). *Leitfaden der Pollenbestimmung für Mitteleuropa und angrenzende Gebiete, Fisch*. Stuttgart., Friedrich Pfeil, München.

Blaauw, M. (2010). Methods and code for 'classical' age-modelling of radiocarbon sequences. *Quaternary Geochronology*, 5, 512–518. DOI: 10.1016/j.quageo.2010.01.002

Brayshaw, D.J., Rambeau, C.M.C. & Smith, S.J. (2011). Changes in Mediterranean climate during the Holocene: insights from global and regional climate modelling. *The Holocene,* 21, 15–31. DOI: 10.1177/0959683610377528

Burjachs, F., Giralt, S., Roca. J.R. (1997). Palinología holocénica y desertización en el Mediterráneo occidental. Ibáñez, J.J., Valero, B.L. & Machado, C. (eds.): In: *El paisaje mediterráneo a través del espacio y del tiempo. Implicaciones en la desertificación*. (pp. 379–394). Geoforma Editores, Logroño, Spain.

Cacho, I., Grimalt, J.O. & Canals, M. (2002). Response of the Western Mediterranean Sea to rapid climatic variability during the last 50 000 years: a molecular biomarker approach. *Journal of Marine Systems*, 33–34, 253–272. DOI: 10.1016/S0924-7963(02)00061-1

Camuera, J., Jiménez-Moreno, G., Ramos-Román, M.J., García-Alix, A., Toney, J.L., Anderson, R.S., Jiménez-Espejo, F.J. … Martínez-Ruiz, F. (2018). Orbital-scale environmental and climatic changes recorded in a new ~ 200 000-year-long multiproxy sedimentary record from Padul, southern Iberian Peninsula. *Quaternary Science Reviews*, 198, 91-114. DOI: 10.1016/j.quascirev.2018.08.014

Camuera, J., Jiménez-Moreno, G., Ramos-Román, M.J., García-Alix, A., Toney, J.L., Anderson, R.S., Jiménez-Espejo, F., ... Carrión, J.S. (2019). Vegetation and climate changes during the last two glacial-interglacial cycles in the western Mediterranean: a new long pollen record from Padul (southern Iberian Peninsula). *Quaternary Science Reviews*, 205, 86–105. DOI: 10.1016/J.QUASCIREV.2018.12.013

Camuera, J., Jiménez-Moreno, G., Ramos-Román, M.J., García-Alix, A., Jiménez-Espejo, F.J., Toney, J.L. & Anderson, R.S. (2021). Chronological control and centennial-scale climatic subdivisions of the last Glacial termination in the western Mediterranean region.

Quaternary Science Reviews, 255, 106814. DOI: 10.1016/j.quascirev.2021.106814

Camuera, J., Ramos-Román, M.J., Jiménez-Moreno, G., García-Alix, A., Ilvonen, L., Ruha, L., Gil-Romera, G., González-Sampériz, P. & Seppä, H. (2022). Past 200 kyr hydroclimate variability in the western Mediterranean and its connection to the African Humid periods. *Scientific Reports*, 12, 9050. DOI: 10.1016/j.quascirev.2021.106814

Carrión, J.S. (2002). Patterns and processes of late Quaternary environmental change in a montane region of southwestern Europe. *Quaternary Science Reviews*, 21, 2047–2066. DOI: 10.1016/S0277-3791(02)00010-0

Carrión, J.S., Sánchez-Gómez, P., Mota, J.F., Yll, R. & Chaín, C. (2003). Fire and grazing are contigent on the Holocene vegetation dynamics of Sierra de Gádor, southern Spain. *The Holocene*, 13, 839–849. DOI: 10.1191/0959683603hl662rp

Carrión, J.S., Fernández, S., Jiménez-Arenas, J.M., Munuera, M., Ochando, J., Amorós, G., Ponce de León, M. … Walker, M.J. (2019). The sequence at Carihuela Cave and its potential for research into Neanderthal ecology and the Mousterian in southern Spain. *Quaternary Science Reviews*, 217, 194-216. DOI: 10.1016/j.quascirev.2019.04.012

Carrión, J.S., Fuentes, N. & González-Sampériz, P. (2007). Holocene environmental change in a montane region of sourthern Europe with a long history of human settlement. *Quaternary Science Reviews*, 26, 1455–1475. DOI: 10.1016/j.quascirev.2007.03.013

Català, A., Cacho, I., Frigola, J., Pena, L.D. & Lirer, F. (2019). Holocene hydrography evolution in the Alboran Sea: a multi-record and multiproxy comparison. *Climate of the Past*, 15, 927–942. DOI: 10.5194/cp-15-927-2019

Cohen, A. S. (2003). *Paleolimnology: The History and Evolution of Lake Systems*. Oxford Academic, New York. USA. DOI: 10.1669/0883-1351(2004)019<0184:BR>2.0.CO;2

Combourieu Nebout, N., Peyron, O., Dormoy, I., Desprat, S., Beaudouin, C., Kotthoff, U. & Marret, F. (2009). Rapid climatic variability in the west Mediterranean during the last 25 000 years from high resolution pollen data. *Climate of the Past*, 5, 503–521. DOI: 10.5194/cp-5-503-2009

Cranwell, P.A. (1984). Lipid geochemistry of sediments from Upton broad, a small productive lake. *Organic Geochemistry*, 7, 25–37. DOI: 10.1016/0146-6380(84)90134-7

Daniau, A.L., Sánchez-Goñi, M.F., Beaufort, L., Laggoun-Défarge, F., Loutre, M.F. & Duprat, J. (2007). Dansgaard–Oeschger climatic variability revealed by fire emissions in southwestern Iberia. *Quaternary Science Reviews*, 26, 1369–1383. DOI: 10.1016/j.quascirev.2007.02.005

Dearing, J. (1999). Magnetic susceptibility. J. Walden, F. Oldfield & J. Smith (eds.): In: *Environmental Magnetism: A Practical Guide*. (pp. 35–62). Quaternary Research Association, London, UK.

Dormoy, I., Peyron, O., Combourieu Nebout, N., Goring, S., Kotthoff, U., Magny, M., & Pross, J. (2009). Terrestrial climate variability and seasonality changes in the Mediterranean region between 15 000 and 4000 years BP deduced from marine pollen records. *Climate of the Past*, 5, 615–632. DOI: 10.5194/cp-5-615-200

Eglinton, T.I. & Eglinton, G. (2008). Molecular proxies for paleoclimatology. *Earth and Planetary Science Letters*, 275, 1–16. DOI: 10.1016/j.epsl.2008.07.012

Faegri, K. & Iversen, J. (1989). *Textbook of Pollen Analysis*. Caldwell. Blackburn Press, New Jersey, USA.

Farquhar, G.D., O'Leary, M.H. & Berry, J.A. (1982). On the relationship between carbon isotope discrimination and the intercellular carbon dioxide concentration in leaves. *Australian Journal of Plant Physiology*, 9, 121–137. DOI: 10.1071/PP9820121

Fernández, S., Fuentes, N., Carrión, J.S., González-Sampériz P., Montoya E., Gil-Romera, G., Vega-Toscano, L.G. & Riquelme, J.A. (2007). The Holocene and upper Pleistocene pollen sequence of Carihuela cave, southern Spain. *Geobios*, 40, 75–90. DOI: 10.1016/j.geobios.2006.01.004

Ficken, K.J. Li, B., Swain, D. & Eglinton, G. (2000). An n-alkane proxy for the sedimentary

input of submerged/floating freshwater aquatic macrophytes. *Organic Geochemistry*, 31, 745–749. DOI: 10.1016/S0146-6380(00)00081-4

Fletcher, W.J. & Sanchez Goñi, M.F. (2008). Orbital- and sub-orbital-scale climate impacts on vegetation of the western Mediterranean basin over the last 48 000 yr. *Quaternary Research*, 70, 451–464. DOI: 10.1016/j.yqres.2008.07.002

Fletcher, W.J., Sanchez Goñi, M.F., Peyron, O. & Dormoy, I. (2010). Abrupt climate changes of the last deglaciation detected in a Western Mediterranean forest record. *Climate of the Past*, 6, 245–264. DOI: 10.5194/cp-6-245-2010

Fletcher, W.J., Debret, M. & Sanchez Goñi, M.F. (2013). Mid-Holocene emergence of a low frequency millennial oscillation in western Mediterranean climate: implications for past dynamics of the North Atlantic atmospheric westerlies. *The Holocene*, 23(2), 153-166. DOI: 10.1177/0959683612460783

García-Alix, A., Jiménez-Moreno, G., Anderson, R.S., Jiménez-Espejo, F. & Delgado-Huertas, A. (2012). Holocene paleoenvironmental evolution of a high-elevation wetland in Sierra Nevada, southern Spain, deduced from an isotopic record. *Journal of Paleolimnology*, 48, 471–484. DOI: 10.1007/s10933-012-9625-2

García-Alix, A., Jiménez-Espejo, F.J., Lozano, J.A., Jiménez-Moreno, G., Martínez-Ruiz, F., García Sanjuán, L., Aranda Jiménez, G. … Anderson, R.S. (2013). Anthropogenic impact and lead pollution throughout the Holocene in southern Iberia. *Science of the Total Environment*, 449, 451-460. DOI: 10.1016/j.scitotenv.2013.01.081

García-Alix, A., Jiménez-Espejo, F.J., Toney, J.L., Jiménez-Moreno, G., Ramos-Román, M.J., Anderson, R.S., Ruano, P. … Kuroda, J. (2017). Alpine bogs of southern Spain show human-induced environmental change superimposed on long-term natural variations. *Scientific Reports*, 7, 7439. DOI: 10.1038/s41598-017-07854-w

García-Alix, A., Jiménez-Espejo, F.J., Jiménez-Moreno, G., Toney, J.L., Ramos-Román, M.J., Camuera, J., Anderson, R.S. … Queralt, I. (2018). Holocene geochemical footprint from Semi-arid alpine wetlands in southern Spain. *Scientific Data*, 5, 180024. DOI: 10.1038/sdata.2018.24

García-Alix, A., Toney, J.L., Jiménez-Moreno, G., Pérez-Martínez, C., Jiménez, L., Rodrigo-Gámiz, M., Anderson, R.S. … Ramos-Román, M.J. (2020). Algal lipids reveal unprecedent warming rates in alpine areas of SW Europe during the Industrial Period. *Climate of the Past*, 16, 245-263.

García-Alix, A., Camuera, J., Ramos-Román, M.J., Toney, J.L., Sachse, D., Schefuß, E., Jiménez-Moreno, G. … Yanes, Y. (2021). Paleohydrological dynamics in the Western Mediterranean during the last glacial cycle. *Global and Planetary Change*, 202, 103527. DOI: 10.5194/cp-16-245-2020

Gehrig-Fasel, J., Guisan, A. & Zimmermann, N.E. (2008). Evaluating thermal treeline indicators based on air and soil temperature using an air-to-soil temperature transfer model. *Ecological Modelling*, 213, 345-355. DOI: 10.1016/j.ecolmodel.2008.01.003

Heegaard, E., Birks, H.J.B. & Telford, R.J. (2005). Relationships between calibrated ages and depth in stratigraphical sequences: an estimation procedure by mixed-effect regression. *The Holocene*, 15, 612–618. DOI: 10.1191/0959683605hl836

Heiri, O., Brooks, S.J., Birks, H.J.B. & Lotter, A.F. (2011). A 274-lake calibration data-set and inference model for chironomid-based summer air temperature reconstruction in Europe. *Quaternary Science Reviews*, 30, 3445–3456. DOI: 10.1016/j.quascirev.2011.09.006

IPCC (2022). *Climate Change 2022: Impacts, Adaptation, and Vulnerability. Contribution of Working Group II to the Sixth Assessment Report of the Intergovernmental Panel on Climate Change*. H.-O. Pörtner, D.C. Roberts, M. Tignor, E.S. Poloczanska, K. Mintenbeck, A. Alegría, M. Craig, S. Langsdorf, S. Löschke, V. Möller, A. Okem, B. Rama (eds.). (pp. 3056). Cambridge University Press. Cambridge University Press, Cambridge, UK and New York, NY, USA. DOI: 10.1017/9781009325844

Jalut, G., Dedoubat, J.J., Fontugne, M. & Otto, T. (2009). Holocene circum-Mediterranean vegetation changes: climate forcing and human

impact. *Quaternary International*, 200, 4–18. DOI: 10.1016/J.QUAINT.2008.03.012

Jiménez-Espejo, F.J., García-Alix, A., Jiménez-Moreno, G., Martínez-Ruiz, F., Anderson, R.S., Rodríguez-Tovar, F.J., Giralt, S. … Pardo-Igúzquiza, E. (2014). Saharan aeolian input and effective humidity variations over Western Europe during the Holocene. *Chemical Geology*, 374-375, 1-12. DOI: 10.1016/j.chemgeo.2014.03.001

Jiménez-Espejo, F.J., Presti, M., Kuhn, G., Mckay, R., Crosta, X., Escutia, C., Lucchi, R.G. … De Santis, L. (2020). Late Pleistocene oceanographic and depositional variations along the Wilkes Land margin (East Antarctica) reconstructed with geochemical proxies in deep-sea sediments. *Global and Planetary Change*, 184, 103045. DOI: 10.1016/j.gloplacha.2019.103045

Jiménez-Moreno, G. & Anderson, R.S. (2012). Holocene vegetation and climate change recorded in alpine bog sediments from the Borreguiles de la Virgen, Sierra Nevada, southern Spain. *Quaternary Research*, 77, 44-53. DOI: 10.1016/j.yqres.2011.09.006

Jiménez-Moreno, G., García-Alix, A., Hernández-Corbalán, M.D., Anderson, R.S. & Delgado-Huertas, A. (2013). Vegetation, fire, climate and human disturbance history in the southwestern Mediterranean area during the late Holocene. *Quaternary Research*, 79, 110-122. DOI: 10.1016/j.yqres.2012.11.008

Jiménez-Moreno, G., Rodríguez-Ramírez, A., Pérez-Asensio, J.N., Carrión, J.S., López-Sáez, J.A., Villarías-Robles, J.J., Celestino-Pérez, S. … León, A. (2015). Impact of late-Holocene aridification trend, climate variability and geodynamic control on the environment from a coastal area in SW Spain. *The Holocene*, 25, 607-617. DOI: 10.1177/0959683614565955

Jiménez-Moreno, G., Anderson, R.S., Ramos-Román, M.J., Camuera, J., Mesa-Fernández, J.M., García-Alix, A., Jiménez-Espejo, F.J. … López-Avilés, A. (2020). The Holocene Cedrus pollen record from Sierra Nevada (S Spain), a proxy for climate change in N Africa. *Quaternary Science Reviews*, 242, 106468. DOI: 10.1016/j.quascirev.2020.106468

Jiménez-Moreno, G., García-Alix, A., Anderson, R.S., Ramos-Román, M.J., Camuera, J., Mesa-Fernández, J.M., Toney, J.L. … Webster, C.E. (2022). Reconstruction of Past Environment and Climate Using Wetland Sediment Records from the Sierra Nevada. R. Zamora & M. Oliva (eds.): In: *The Landscape of the Sierra Nevada*. (pp. 95-114). Springer Nature Switzerland AG. DOI: 10.1007/978-3-030-94219-9_7

Jiménez-Moreno, G., Heiri, O., García-Alix, A., Anderson, R.S., Jiménez-Espejo, F.J., López-Blanco, C., Jiménez, L. … Camuera, J. (2023a). Holocene summer temperature reconstruction based on a chironomid record from Sierra Nevada, southern Spain. *Quaternary Science Reviews*, 319, 108343. DOI: 10.1016/j.quascirev.2023.108343

Jiménez-Moreno, G., López-Avilés, A., García-Alix, A., Ramos-Román, M.J., Camuera, J., Mesa-Fernández, J.M., Jiménez-Espejo, F.J. … Anderson, R.S. (2023b). Laguna Seca sediments reveal environmental and climate change during the latest Pleistocene and Holocene in Sierra Nevada, southern Iberian Peninsula. *Palaeogeography, Palaeoclimatology, Palaeoecology*, 631, 111834. DOI: 10.1016/j.palaeo.2023.111834

Linstädter, A. & Zielhofer, C. (2010). Regional fire history shows abrupt responses of Mediterranean ecosystems to centennial-scale climate change (Olea–Pistacia woodlands), NE Morocco. *Journal of Arid Environments*, 74, 101–110. DOI: 10.1016/j.jaridenv.2009.07.006

López-Avilés, A., García-Alix, A., Jiménez-Moreno, G., Anderson, R.S., Toney. J.L., Mesa-Fernández, J.M. & Jiménez-Espejo, F.J. (2021). Latest Holocene paleonvironmental and paleoclimate reconstruction from an alpine bog in the Western Mediterranean region: The Borreguil de los Lavaderos de la Reina record (Sierra Nevada). *Palaeogeography, Palaeoclimatology, Palaeoecology*, 573, 110434.

López-Avilés, A., Jiménez-Moreno, G., García-Alix, A., García-García, F., Camuera, J., Anderson, R.S., Sanjurjo-Sánchez, J. .. Carrión, J.S. (2022). Post-glacial evolution of alpine environments in the western Mediterranean region: The Laguna Seca record. *Catena*, 211, 106033. DOI: 10.1016/j.palaeo.2021.110434

López-Blanco, C., García-Alix, A., Jiménez-Moreno, G., Rodrigo-Gámiz, M. & Anderson, R.S. (2024). Climatic fluctuations over the Holocene in southern Iberia (Sierra Nevada, Spain) reconstructed by fossil cladocerans. *Palaeogeography, Palaeoclimatology, Palaeoecology*, 638, 111989. DOI: 10.1016/j.palaeo.2023.111989

López-Blanco, C., García-Alix, A., Sánchez-Almazo, I., Jiménez-Moreno, G. & Anderson, R.S. (2025). Holocene changes in moisture source and temperatura revealed by the oxygen isotopic composition of fossil *Daphnia* ephippia in Sierra Nevada, southern Spain. *Catena*, 254, 108984. DOI: 10.1016/j.catena.2025.108984

Lowe, J.J., Rasmussen, S.O., Bjoerck, S., Hoek, W.Z., Steffensen, J.P., Walker, M.J.C. … the INTIMATE group. (2008). Synchronisation of palaeoenvironmental events in the North Atlantic region during the Last Termination: a revised protocol recommended by the INTIMATE group. *Quaternary Science Reviews*, 27, 6-17. DOI: 10.1016/j.quascirev.2007.09.016

Löwemark, L., Chen, H.-F., Yang, T.-N., Kylander, M., Yu, E.F., Hsu, Y.W., Lee, T.Q. … Jarvis, S.W. (2011). Normalizing XRF-scanner data: A cautionary note on the interpretation of high-resolution records from organic-rich lakes. *Journal of Asian Earth Sciences*, 40, 1250–1256. DOI: 10.1016/j.jseaes.2010.06.002

Malanson, G.P., Resler, L.M., Butler, D.R. & Fagre, D.B. (2019). Mountain plant communities: uncertain sentinels?. *Progress in Physical Geography*, 43, 521-543. DOI: 10.1177/0309133319843873

Manzano, S., Carrión, J.S., López-Merino, L., Jiménez-Moreno, G., Toney, J., Armstrong, H., Anderson, R. S. … Sánchez-Mata, D. (2019). A palaeoecological approach to understanding the past and present of Sierra Nevada, a Southwestern European biodiversity hotspot. *Global and Planetary Change*, 175, 238-250. DOI: 10.1016/j.gloplacha.2019.02.006

Martín-Puertas, C., Valero-Garcés, B.L., Brauer, A., Mata, M.P., Delgado-Huertas, A. & Dulski, P. (2009). The Iberian-Roman Humid Period (2600-1600 cal yr BP) in the Zoñar lake varve record (Andalucía, southern Spain). *Quaternary Research*, 71, 108-120. DOI: 10.1016/j.yqres.2008.10.004

Martínez-Ruiz, F., Kastner, M., Gallego-Torres, D., Rodrigo-Gámiz, M., Nieto-Moreno, V. & Ortega-Huertas, M. (2015) Paleoclimate and paleoceanography over the past 20 000 yr in the Mediterranean Sea Basins as indicated by sediment elemental proxies. *Quaternary Science Reviews*, 107, 25-46. DOI: 10.1016/j.quascirev.2014.09.018

Mesa-Fernández, J.M., Jiménez-Moreno, G., Rodrigo-Gámiz, M., García-Alix, A., Jiménez-Espejo, F. J., Martínez-Ruiz, F., Anderson, R. S. … Ramos-Román, M.J. (2018). Vegetation and geochemical response to Holocene rapid climate change in the Sierra Nevada (southeastern Iberia): the Laguna Hondera record. *Climate of the Past*, 14, 1687-1706. DOI: 10.5194/cp-14-1687-2018

Meijer, P.Th. & Tuenter, E. (2007). The effect of precession-induced changes in the Mediterranean freshwater budget on circulation at shallow and intermediate depth. *Journal of Marine Systems*, 68, 349–365. DOI: 10.1016/j.jmarsys.2007.01.006

Meyers, P.A. & Ishiwatari, R. (1993). Lacustrine Organic Geochemistry—An Overview of Indicators of Organic Matter Sources and Diagenesis in Lake Sediments. *Organic Geochemistry*, 20(7), 867–900. DOI: 10.1016/0146-6380(93)90100-P

Meyers P.A. (1994). Preservation of elemental and isotopic source identification of sedimentary organic matter. *Chemical Geology*, 113, 289–302. DOI: 10.1016/0009-2541(94)90059-0

Meyers, P.A. & Teranes, J.L. (2001). Sediment organic matter. W.M. Last & J.P. Smol (eds.): In: *Tracking environmental changes using lake sediments*, vol 2. (pp 239–270). Kluwer, Dordrecht.

Moreno, A., Pérez, A., Frigola, J., Nieto-Moreno, V., Rodrigo-Gámiz, M., Martrat, B., González-Sampériz, P. … Valero-Garcés, B. (2012). The Medieval Climate Anomaly in the Iberian Peninsula reconstructed from marine and lake records. *Quaternary Science Reviews*, 42, 16–32. DOI: 10.1016/j.quascirev.2012.04.007

O'Leary, M.H. (1988). Carbon isotopes in photosynthesis. *Bioscience*, 38, 328–336. DOI: 10.2307/1310735

Oliva, M., Gómez-Ortiz, A., Palacios, D., Salvador-Franch, F., Andrés, N., Tanarro, L.M., Fernández-Fernández, J.M. & Barriocanal, C. (2020). Multiproxy reconstruction of Holocene glaciers in Sierra Nevada (south Spain). *Mediterranean Geoscience Reviews*, 2, 5-19. DOI: 10.1007/S42990-019-00008-2

Palacios, D., Gómez-Ortiz, A., Andrés, N., Salvador, F. & Oliva, M. (2016). Timing and new geomorphologic evidence of the last deglaciation stages in Sierra Nevada (southern Spain). *Quaternary Science Reviews*, 150, 110–129. DOI: 10.1016/j.quascirev.2016.08.012

Páscoa, P., Gouveia, C.M., Russo, A. & Trigo, R.M. (2017). Drought trends in the Iberian Peninsula over the last 112 years. *Advances in Meteorology*, 2017, 4653126. DOI: 10.1155/2017/4653126

Pausas, J.G. & Fernández-Muñoz, S. (2012). Fire regime changes in the western Mediterranean basin: from fuel limited to drought-driven fire regime. *Climate Change*, 110, 215–226. DOI: 10.1007/s10584-011-0060-6

Ramos-Román, M.J., Jiménez-Moreno, G., Anderson, R.S., García-Alix, A., Toney, J.L., Jiménez-Espejo, F.J. & Carrión, J.S. (2016). Centennial-scale vegetation and North Atlantic Oscillation changes during the late Holocene in the western Mediterranean. *Quaternary Science Reviews*, 143, 84-95. DOI: 10.1016/j.quascirev.2016.05.007

Ramos-Román, M.J., Jiménez-Moreno, G., Camuera, J., García-Alix, A., Anderson, R.S., Jiménez-Espejo, F.J. & Carrión, J.S. (2018a). Holocene climate aridification trend and human impact interrupted by millennial and centennial-scale climate fluctuations from a new sedimentary record from Padul (Sierra Nevada, southern Iberian Peninsula). *Climate of the Past*, 14, 117–137. DOI: 10.5194/cp-14-117-2018

Ramos-Román, M.J., Jiménez-Moreno, G., Camuera, J., García-Alix, A., Anderson, R.S., Jiménez-Espejo, F.J., Sachse, D. … Yanes, Y. (2018b). Millennial-scale cyclical environment and climate variability during the Holocene in the western Mediterranean region deduced from a new multiproxy analysis from the Padul record (Sierra Nevada, Spain). *Global and Planetary Change*, 168, 35-53. DOI: 10.1016/j.gloplacha.2018.06.003

Ramos-Román, M.J., Jiménez-Moreno, G., Anderson, R.S. García-Alix, A., Camuera, J., Mesa-Fernández, J.M. & Manzano, S. (2019). Climate controlled historic olive tree occurrences and olive oil production in southern Spain. *Global and Planetary Change*, 182, 102996. DOI: 10.1016/j.gloplacha.2019.102996

Reille, M. (1992). *Pollen et Spores d'Europe et Afrique du Nord*. Laboratoire de Botanique Historique et Palynologie, Marseille, France.

Reimer, P., Austin, W., Bard, E., Bayliss, A., Blackwell, P., Bronk Ramsey, C. & Talamo, S. (2020). The IntCal20 northern hemisphere radiocarbon age calibration curve (0–55 cal kBP). *Radiocarbon*, 62 (4), 725–757. DOI: 10.1017/RDC.2020.41

Renssen, H., Brovkin, V., Fichefet, T. & Goosse, H. (2003). Holocene climate instability during the termination of the African Humid Period. *Geophysical Research Letters*, 30, 1184. DOI: 10.1029/2002GL016636

Rodrigo-Gámiz, M., Martínez-Ruiz, F., Jiménez-Espejo, F.J., Gallego-Torres, D., Nieto-Moreno, V., Romero, O. & Ariztegui, D. (2011). Impact of climate variability in the western Mediterranean during the last 20 000 years: oceanic and atmospheric responses. *Quaternary Science Reviews*, 30, 2018-2034. DOI: 10.1016/j.quascirev.2011.05.011

Rodrigo-Gámiz, M., Martínez-Ruiz, F., Rampen, S.W., Schouten, S. & Sinninghe Damsté, J.S. (2014). Sea surface temperature variations in the western Mediterranean Sea over the last 20 kyr: a dual-organic proxy (UK′37 and LDI) approach. *Paleoceanography*, 29, 87–98. DOI: 10.1002/2013PA002466

Rodrigo-Gámiz, M., García-Alix, A., Jiménez-Moreno, G., Ramos-Román, M.J., Camuera, J., Toney, J.L., Sachse, D. ... Sinninghe Damsté, J.S. (2022). Paleoclimate reconstruction of the last 36 kyr based on branched glycerol dialkyl glycerol tetraethers in the Padul palaeolake record (Sierra Nevada, southern Iberian Peninsula). *Quaternary Science Re-*

views, 281, 107434. DOI: 10.1016/j.quascirev.2022.107434

Russell, J.M., Hopmans, E.C., Loomis, S.E., Liang, J. & Sinninghe Damste, J.S. (2018). Distributions of 5- and 6-methyl branched glycerol dialkyl glycerol tetraethers (brGDGTs) in East African lake sediment: effects of temperature, pH, and new lacustrine paleotemperature calibrations. *Organic Geochemistry*, 117, 56-69. DOI: 10.1016/j.orggeochem.2017.12.003

Samartin, S., Heiri, O., Joos, F., Renssen, H., Franke, J., Brönnimann, S. & Tinner, W. (2017). Warm Mediterranean mid-Holocene summers inferred from fossil midge assemblages. *Nature Geosciences*, 10, 207–212. DOI: 10.1038/ngeo2891

Sarmaja-Korjonen, K. (2004). Chydorid ephippia as indicators of past environmental changes - A new method. *Hydrobiologia*, 526, 129–136. DOI: 10.1023/B:HYDR.0000041595.08121.ab

Sarmaja-Korjonen, K. (2003). Chydorid ephippia as indicators of environmental change - Biostratigraphical evidence from two lakes in southern Finland. *The Holocene*, 13, 691–700. DOI: 10.1191/0959683603hl655rp

Snowball, I. & Sandgren, P. (2001). Application of mineral magnetic techniques to paleolimnology. W.M. Last, J.P. Smol (eds.): In: *Tracking Environmental Changes Using Lake Sediments*, vol 2. (pp. 217–237). Kluwer Academic Publishers, Dordrecht. DOI: 10.1007/0-306-47670-3_8

Sousa, P.M., Trigo, R.M., Pereira, M.G., Bedia, J. & Gutierrez, J.M. (2015). Different approaches to model future burnt area in the Iberian Peninsula. *Agricultural and Forest Meteorology*, 202, 11–25. DOI: 10.1016/j.agrformet.2014.11.018

Sousa, P.M., Barriopedro, D., Ramos, A.M., García-Herrera, R., Espírito-Santo, F. & Trigo, R.M. (2019). Saharan air intrusions as a relevant mechanism for Iberian heatwaves: The record breaking events of August 2018 and June 2019. *Weather and Climate Extremes*, 26, 100224. DOI: 10.1016/j.wace.2019.100224

Szeroczyńska, K. & Sarmaja-Korjonen, K. (2007). *Atlas of subfossil cladocera from central and northern Europe*. Friends of the Lower Vistula Society. 84 pp.

Talbot, M.R. (2001). Nitrogen isotopes in palaeolimnology. W.M. Last, J.P. Smol (eds.): In: *Tracking environmental changes using lake sediments: physical and chemical techniques*. (pp. 401–439). Kluwer, Dordrecht. DOI: 10.1007/0-306-47670-3_15

Thuiller, W., Lavorel, S., Araujo, M.B., Sykes, M.T. & Prentice, I.C. (2005). *Climate change threats to plant diversity in Europe*. PNAS, 102, 8245-8250. DOI: 10.1073/pnas.0409902102

Toney, J.L., García-Alix, A., Jiménez-Moreno, G., Anderson, R.S., Moossen, H. & Seki, O. (2020). New insights into Holocene hydrology and temperature from lipid biomarkers in western Mediterranean alpine wetlands. *Quaternary Science Reviews*, 240, 106395. DOI: 10.1016/j.quascirev.2020.106395

Trouet, V., Esper, J., Graham, N.E., Baker, A., Scourse, J.D. & Frank, D.C. (2009). Persistent positive north Atlantic oscillation mode dominated the Medieval climate anomaly. *Science*, 324, 78–80. DOI: 10.1126/science.1166349

Tuenter, E., Weber, S.L., Hilgen, F.J. & Lourens, L.J. (2003). The response of the African summer monsoon to remote and local forcing due to precession and obliquity. *Global and Planetary Change*, 36, 219–235. DOI: 10.1016/S0921-8181(02)00196-0

Valle, F. (2003). *Mapa de Series de Vegetación de Andalucía*. Editorial Rueda S.I., Madrid, Spain.

Verbruggen, F., Heiri, O., Reichart, G.J., de Leeuw, J.W., Nierop, K.G.J. & Lotter, A.F. (2010). Effects of chemical pretreatments on δ18O measurements, chemical composition, and morphology of chironomid head capsules. *Journal of Paleolimnology*, 43, 857–872. DOI: 10.1007/s10933-009-9374-z

Webster, C.E. (2018). Late-Pleistocene and Holocene record of fire at Padul peat bog (Granada, Spain). (MS Dissertation, Northern Arizona University, USA).

Whitlock, C. & Anderson, R.S. (2003). Fire history reconstructions based on sediment records from lakes and wetlands. T.T. Veblen, W.L. Baker, G. Montenegro, T.W. Swetnam

(eds.): In: *Fire and Climatic Change in Temperate Ecosystems of the Americas*, vol 160. (pp. 3–31). Springer-Verlag, New York. DOI: 10.1007/0-387-21710-X_1

Weltje, G.J. & Tjallingii, R. (2008). Calibration of XRF core scanners for quantitative geochemical logging of sediment cores: Theory and application. *Earth and Planetary Science Letters*, 274, 423–438. DOI: 10.1016/j.epsl.2008.07.054

Wolfe, B.B., Edwards, T.W.D., Beuning, K.R.M. & Elgood, R.J. (2001). Carbon and oxygen isotope analysis of lake sediment cellulose: methods and applications. In: W.M. Last & J.P. Smol (eds.). In: *Tracking environmental changes using lake sediments: physical and chemical techniques*. (pp. 373–400). Kluwer, Dordrecht. DOI: 10.1007/0-306-47670-3_14

Zielhofer, C., Köhler, A., Mischke, S., Benkaddour, A., Mikdad, A. & Fletcher, W. J. (2019). Western Mediterranean hydro-climatic consequences of Holocene ice-rafted debris (Bond) events. *Climate of the Past*, 15, 463–475. DOI: 10.5194/cp-15-463-2019